Modeling of Adaptive Neuro-Fuzzy Inference System (ANFIS)- based MPPT controller for a solar Photovoltaic Powered Water Pumping System

Habtewold Abera Bikila

A Thesis Submitted to the Department of Power and Control Engineering

College of Electrical Engineering and Computing

Office of Graduate Studies

Adama Science and Technology University

October, 2025

Adama, Ethiopia

Modeling of Adaptive Neuro-Fuzzy Inference System (ANFIS)- based MPPT controller for a solar Photovoltaic Powered Water Pumping system

Habtewold Abera Bikila

Advisor

Dr. Negasa Muleta

A Thesis Submitted to the Department of Power and Control Engineering

College of Electrical Engineering and Computing

Office of Graduate Studies

Adama Science and Technology University

October, 2025

Adama, Ethiopia

DECLARATION

I thus certify that my master's thesis, **"Modeling of Adaptive Neuro-Fuzzy Inference System (ANFIS)-based MPPT controller for a solar Photovoltaic Powered Water Pumping system,"** is my original work. To put it another way, it hasn't been submitted to another university for the purpose of receiving a degree, diploma, or certificate. Every single source of material used in this thesis has been appropriately cited.

Habtewold Abera Bikila		Oct 16, 2025
Name of the student	Signature	Date

RECOMMENDATION

I certify that, in my capacity as thesis advisor, I have read the revised thesis, **"Modeling of Adaptive Neuro-Fuzzy Inference System (ANFIS)-based MPPT controller for a solar Photovoltaic Powered Water Pumping system,"** which was created under my/our guidance by **Habtewold Abera** and turned in as a partial completion of the requirements for the master's degree in power system engineering.

Therefore, in compliance with the applicable procedures, I suggest presenting the revised thesis to the department.

Dr. Negasa Muleta		Oct 16 ,2025
Advisor	Signature	Date

APPROVAL PAGE

I, the advisor of the thesis entitled **"Modeling of Adaptive Neuro-Fuzzy Inference System (ANFIS)-based MPPT controller for a solar Photovoltaic Powered Water Pumping system"** and developed by **Habtewold Abera Bikila,** hereby certify that the recommendation and suggestions made by the board of examiners are appropriately incorporated into the final version of the thesis.

Dr. Negasa Muleta		Oct 16 ,2025
Advisor	Signature	Date

We, the undersigned, members of the Board of Examiners of the thesis by **Habtewold Abera Bikila,** have read and evaluated the thesis entitled **"Modeling of Adaptive Neuro-Fuzzy Inference System (ANFIS)-based MPPT controller for a solar Photovoltaic Powered Water Pumping system"** and examined the candidate during open defense. This is, therefore, to certify that the thesis is accepted for partial fulfillment of the degree requirement of the Master of Science in Power System Engineering.

Chairperson	Signature	Date
Internal Examiner	Signature	Date
Dr. Yeshitela Shiferaw		Oct 16,2025
External Examiner	Signature	Date

Final approval and acceptance of the thesis is contingent upon submission of its final copy to the Office of Postgraduate Studies (OPGS) through the Department Graduate Council (DGC) and School Graduate Committee (SGC).

Department Head	Signature	Date
college Dean	Signature	Date
Office of Postgraduate Studies, Dean	Signature	Date

ACKNOWLEDGMENT

First and foremost, I want to give thanks and praise to the Almighty Lord for guiding me through this challenging but incredibly motivating task and for giving me the patience and ideas I needed to finish this thesis. Then, I want to sincerely thank and appreciate my adviser, **Dr. Negasa Muleta,** for all of his help and support during this process of personal development. His patience and encouragement have allowed me to reach my full potential in both my academic and professional endeavors. Finally, I would want to thank my wife, **Mrs. Abonesh Biruk,** for supporting me through every challenge.

I am grateful to all Adama Science and Technology University's Electrical Power and Control Engineering department members. I would like to thank all my friends and fellow students. Thank you for sharing your pleasure and need for knowledge with me and for always being willing to assist me in working through the occasional threatening problems.

Finally, I would like to thank Adama Science and Technology University for giving me this glorious chance to study my master's degree at one of the Prestigious Universities in Ethiopia.

TABLE OF CONTENTS

LIST OF TABLES

LIST OF FIGURES

LIST OF ABBREVIATIONS

AC	Alternating Current
D	Duty cycle ration
DC	Direct Current
FIS	Fuzzy Inference System
ANFIS	Adaptive neuro fuzzy inference system
I*mp*	Maximum power point current at reference condition
IRC	International Rescue Committee
ISE	Integral of square error
Ipv	Output current of the solar cell
Isc	Short Circuit current
MPP	Maximum Power Point
MPPT	Maximum Power Point Tracking
IC	Incremental conductance
IGBT	Insulated gate bipolar transistor
KW	Kilowatt
MATLAB	Matrix laboratory
PV	Photovoltaic
PG	Power generation
P&O	Perturb and observe
O&M	Operation and maintenance
NASA	National Aeronautics and space administration

LIST OF SYMBOLS

a	Diode ideality factor
I_d	Diode saturation current,
I_{pv}	Light generated current of the photovoltaic cell
I_{scn}	Short-circuit current at the nominal condition
N_p	Number of cells connected in parallel
N_S	Number of cells connected in series
R_p	Shunt resistance (Ω)
R_S	Series resistance (Ω)
V_d	The voltage across the diode:
$Vocn$	Open circuit current at the nominal condition
ΔT	Deviation from the nominal temperature in Kelvin
G	Actual irradiance in W/m2
g	Gravity
K	Boltzmann constant (1.38 ×10-23) JK-1
q	Electronic charge (1.602 ×10-19)
Q	Water Discharge Rate
T	Module operating temperature in Kelvin
ρ	Water Density

ABSTRACT

This work develops and simulates an adaptive neuro-fuzzy inference system (ANFIS) controller for maximum power point tracking (MPPT) in a photovoltaic (PV)-driven water pumping application, comparing its performance under dynamic irradiance conditions to the traditional Perturb & Observe (P&O) algorithm. The study addresses delayed response time and reduced efficiency in solar PV-powered Permanent Magnet Synchronous Motor (PMSM) drive systems for irrigation. The PV array's DC output is converted to AC for the PMSM drive via a DC-AC inverter, with speed management achieved through field-oriented controllers (FOCs) that compare the motor's actual speed to a reference. Simulation results in MATLAB/Simulink demonstrate that the controller significantly improves the system's speed responsiveness, reduces harmonic distortions, and delivers enhanced power to the irrigation load. Under fluctuating irradiance, the ANFIS-based MPPT increased output power by 12.5% compared to P&O, achieving a maximum power output of 270 kW at 480 V and 10 A from the PV system, outperforming the P&O approach which produced 240 kW at 475 V and 9.5 A, thereby demonstrating superior power extraction capabilities.

Keywords: ANFIS, P&O, MATLAB, solar photovoltaic, and maximum power point tracking

CHAPTER ONE

1. INTRODUCTION

1.1 Background of the Study

As global food consumption steadily rises, rapid technological advancement in food production is becoming increasingly essential. Food insecurity is still a big issue in many developing nations. Increasing crop yields through technology is essential for Ethiopia, whose economy is based primarily on agriculture. However, much of Ethiopian agriculture depends on unpredictable rainfall patterns. Climate change, driven by global warming, has made these rain-fed systems even more unstable. As a result, the country has increasingly turned to irrigation to meet the growing demand for food.

According to the 2023 United Nations World Water Development Report, around 1.2 billion people, or one-fifth of the world's population, reside in regions that physically lack access to water. Additionally, roughly a quarter of the world's population resides in developing regions that frequently struggle with water shortages. Since the early days of civilization, securing clean drinking water and meeting agricultural needs have been persistent challenges.

In regions where grid power is accessible, AC-powered water pumping systems offer a low-cost, low-maintenance solution. However, many rural communities are situated far from the existing power grid, making it prohibitively expensive to install transformers and transmission lines. To address this, diesel-powered pumps have been deployed in remote areas. While these systems are easy to set up and transport, they have limitations including high operational costs, fuel supply issues, and the need for regular maintenance (A. Abubakar and S. Paulo, no. August 2023).

Furthermore, diesel fuel is often expensive and not always available in isolated rural communities. Even when available, transporting fuel to remote villages can be a logistical challenge due to poor infrastructure and lack of roads (Barton). Additionally, the burning of fossil fuels significantly contributes to climate change, with CO_2 emissions being a major concern. Therefore, reducing these emissions is a global priority.

Renewable energy technologies offer a promising alternative. Not only are they often cheaper than fossil fuels, but they also support sustainable development goals. The integration of

renewable sources, especially solar energy, is made possible by advancements in power electronics and digital control technologies. These innovations are key to the ongoing global shift toward cleaner energy systems.

Access to clean water plays a critical role in social, economic, and environmental sustainability. It is essential for drinking, sanitation, agriculture, and ecosystem preservation. Eco-friendly technologies for water delivery, such as remote water pumping systems, are becoming increasingly important. These systems can serve as the foundation for more advanced solutions like desalination and water purification. Solar photovoltaic (PV) energy, in particular, holds great promise for powering such systems, and continued research in this area is essential.

Solar energy presents a viable solution to the twin challenges of energy scarcity and environmental degradation. Achieving sustainable development requires the implementation of strategies that enhance energy efficiency and lower greenhouse gas emissions (Li, 2022). In regions that are both economically disadvantaged and arid, delivering drinking water using sustainable energy sources is both an environmental and humanitarian imperative. Without access to essential services, these communities risk becoming dependent on aid, losing productivity, or even facing depopulation. Solar-powered water pumping systems and PV generation can offer lasting solutions to these challenges.

These solar water pumps can be used for irrigation, watering animals, and providing water to houses and villages in remote areas. Most PV water pumping systems use DC motors that are directly connected to solar panels. Although straightforward in design, these systems often suffer from inefficiencies and frequent breakdowns. Systems using AC motors driven by inverters tend to offer better performance. Permanent magnet synchronous motor, in particular, are preferred for their durability, efficiency, and ease of maintenance.

Today, much research focuses on optimizing the use of renewable energy sources. Among them, solar PV technology is widely recognized due to its numerous benefits. Unlike traditional energy sources, solar panels harness a free and unlimited energy source, produce no emissions, and require minimal upkeep. The photovoltaic effect is how solar cells generate electricity by directly converting sunlight (Kenu E. sarah, 2020).

Choosing the right location for such systems is a critical part of project planning. Despite this, many designers underestimate the significance of proper site selection when designing PV

water pumping solutions. Even the most advanced system cannot function effectively if the water source is inconsistent or inadequate.

In this study, the site was chosen based on water availability, demand for intended uses, and proximity to reliable water sources. The selected location was Amude Kebele, in Dodota Woreda of Ethiopia's Oromia region specifically in the Arsi Zone, near Lake Batu. This lake is one of Ethiopia's prominent freshwater bodies within the Rift Valley and is located approximately 70 km from Adama. Lake Batu spans roughly 440 square kilometers, stretching 31 kilometers in length and 20 kilometers in width, with a maximum depth of nine meters. The lake sits at an elevation of 1,636 meters above sea level, making it a promising source for sustainable water supply initiatives.

1.2 Statement of the problem

Conventional MPPT techniques, such as Perturb and Observe (P&O), are straightforward but often suffer from slow response and oscillations around the maximum power point under rapidly changing environmental conditions. There is a growing need for intelligent, adaptive control techniques that can enhance tracking accuracy and system performance.

By merging the decision-making logic of fuzzy systems with the learning powers of neural networks, the Adaptive Neuro-Fuzzy Inference System (ANFIS) presents a viable remedy. However, there is limited research on the integration and modeling of ANFIS-based MPPT controllers specifically for solar PV-powered water pumping applications. Therefore, a comprehensive study is needed to develop and evaluate an ANFIS-based MPPT controller that can improve energy extraction, ensure stable water pumping, and support sustainable water access in off-grid areas.

Overall the statement correctly identifies the global and local challenges related to solar powered water pumping systems, particularly

- ❖ Intermittent solar irradiance and temperature affecting efficiency.
- ❖ Limitations of traditional MPPT technique (e.g., perturb & observe).
- ❖ The potential of ANFIS based MPPT to enhance performance.
- ❖ Lack of research on ANFIS in solar PV water applications.

The proposed site Amude was selected due to:

- Close proximity to Lake Batu (consistent water source).

- High solar irradiance levels (~5.47 kWh/m²/day).
- Agricultural demand (maize crop irrigation).
- Remote/off-grid location suitable for solar pumping.

1.3 Objectives of the study

1.3.1General objective

To design, model and simulate an Adaptive Neuro-Fuzzy Inference System (ANFIS)_based Maximum Power Point Tracking (MPPT) controller for solar PV _ powered water pumping system, with the goal of enhancing power conversion efficiency, reliability, and stability under varying environmental conditions applications in off-grid and remote locations.

1.3.2 Specific objectives

- ✓ To analyze the solar resource potential and water pumping demand for the selected off-grid site.
- ✓ To design and size a solar PV –powered water pumping system including PV array, converter, inverter and motor
- ✓ To develop and implement both ANFIS-based and perturb and observe (P&O) MPPT controller in MATLAB/Simulink
- ✓ To compare the performance of the ANFIS-based MPPT controller with the conventional P&O method.
- ✓ To simulate the system under varying irradiance and temperature condition and evaluate performance indicators such as tracking efficiency, response time, and output power stability.
- ✓ To assess the feasibility of the proposed ANFIS-based system for reliable and sustainable water supply in rural, off grid environments.

1.4 Significance of the Study

In rural and off-grid settings, where access to clean water and dependable electricity is frequently limited, this study is crucial to the advancement of sustainable water pumping solutions. By simulating an Adaptive Neuro-Fuzzy Inference System (ANFIS)-based

Maximum Power Point Tracking (MPPT) controller and comparing it with the conventional Perturb and Observe (P&O) method, the study aims to improve the responsiveness and efficiency of solar photovoltaic (PV) powered water pumping systems.

Consistent water delivery with lower energy losses is ensured by the suggested intelligent control strategy, which improves energy extraction from solar panels under various climatic situations. By promoting renewable energy technology, this helps not only alleviate the shortage of electricity and water but also advances the more general objectives of environmental sustainability, rural development, and climate change mitigation.

1.5 Scope of the Study

The modeling, simulation, and performance evaluation of an ANFIS-based MPPT controller for a solar photovoltaic (PV)-powered water pumping system are the main objectives of this study. Only the design and implementation of the ANFIS controller in a simulated environment, like MATLAB/Simulink, is covered, and performance is evaluated in comparison to the traditional Perturb and Observe (P&O) MPPT algorithm.

The study largely involves on the output power of the PV system, enhancing MPPT efficiency, and assuring steady operation of the water pump under fluctuating solar irradiance and temperature circumstances. It does not involve hardware implementation or cost analysis, but provides a strong theoretical and simulation-based framework for potential practical applications in rural and off-grid contexts.

1.6. Methodology

The proposed methodology consists of the following steps:

Literature Review Analyze every study, journal article, conference paper, and technical report on Maximum Power Point Tracking (MPPT) methods that are currently available. Pay special attention to controllers that use the Adaptive Neuro-Fuzzy Inference System (ANFIS) and Perturb & Observe (P&O) in solar photovoltaic (PV) water pumping settings.

Data Collection: For rural or remote areas, gather pertinent input parameters such as solar irradiation, temperature fluctuations, PV panel specs, water pump characteristics, and normal daily water demand profiles. Modeling and controller design are based on these datasets.

Data Analysis: Examine the environmental and system data gathered to comprehend the fluctuations in the availability of solar resources and how they affect PV power output and pumping needs. This aids in evaluating the appropriateness of sophisticated MPPT control schemes.

System Design and Modeling: Develop a simulation model of the solar PV-powered water pumping system in MATLAB/Simulink The suggested ANFIS-based MPPT controller and the traditional P&O algorithm will be implemented in order to control power output and guarantee the best possible system performance.

Performance Evaluation: Simulate and Examine how well the P&O and ANFIS-based controllers function in various environmental settings.

Conclusion and Future Work: Summarize the simulation results to highlight the advantages of the ANFIS-based controller over the traditional method. Discuss the implications for real-world deployment and suggest areas for future research, such as hardware implementation and integration with hybrid renewable energy systems.

1.7 Organization of the Thesis

There are five chapters that make up this thesis. The chapter's descriptions are presented as shown below:

Chapter one is the introductory part of the work which is comprised by background, statement of the problem, objective of the study, significance of the research, scope of the study etc. are well presented and discussed.

Chapter two presents the literature review and theoretical backgrounds related to the PV system, MPPT and the method of algorithms used.

Chapter three depicts the methodology and system design with the controller models.

Chapter four presents and discusses on different comparison results of the system and simulations using MATLAB.

Chapter five forwards final conclusions and recommendations based on the research results.

CHAPTER TWO
LITERATURE REVIEW AND THEORETICAL BACKGROUNDS

2.1 Literature reviews

A variety of methods have been proposed to lower energy and power losses in distribution networks and enhance the voltage profile. While some of these algorithms assume a fixed load, others are constructed with the idea that the load changes. While a lesser percentage of the research examined reconfiguration for both goals at the same time, many of these studies concentrated on employing reconfiguration techniques to minimize losses or place compensation devices in the system in the best possible way.

In (Z. Boumous and S. Boumous, 2024) examined the application of a Gravitational Search Algorithm (GSA) to a photovoltaic (PV) micro grid system's Maximum Power Point Tracking (MPPT) controller using the Adaptive Neuro-Fuzzy Inference System (ANFIS). To optimize power output, the primary goal is to efficiently monitor the PV array's maximum power point. The goal of this clever control approach is to raise grid-connected PV systems' efficiency.

In (M. Hassan, March, 2022.) introduced an enhanced ANFIS-based MPPT controller designed for standalone PV systems, addressing the challenge of data acquisition for training. Without the use of a PI controller, it directly modifies the duty cycle of the boost converter and generates accurate training data using a multi-variable step P&O algorithm. When compared to ANN and FLC approaches, simulation results show that the suggested ANFIS-MPPT is more accurate and efficient at tracking the maximum power point under various scenarios.

In (M. Pa, 2024) Provide a smart fault detection system based on ANFIS to quickly detect anomalous activity and improve the dependability of grid-connected PV systems. The system can differentiate between normal and different fault conditions in the PV array, power electronics, and inverter after being educated on a large amount of real-time experimental data. When compared to other machine learning techniques, this ANFIS technology provides a more effective and straightforward solution for PV system maintenance due to its greater accuracy (95.4%) and robustness.

In (K. Chnini, 2025,) suggest a new hybrid ANFIS-RTSMC MPPT technique for a water pumping system that uses an induction motor drive and is powered by PV, diesel, and batteries. The tactic blends ANFIS's fast response with RTSMC's robustness to ensure stable power extraction and resilience against irradiance changes and parameter variations. Simulations validate this two-stage PV setup, demonstrating superior MPPT efficiency and robust operation under diverse conditions.

In (E. E. Hsduwphqw, 2024) stated an ANFIS-based MPPT technique for a solar PV and battery-driven brushless DC motor water pumping system, incorporating a SEPIC converter for soft starting. A bidirectional buck-boost converter enables automatic battery switching for power during off-peak times or bad weather, with the BLDC motor speed controlled by a PWM inverter. MATLAB/SIMULINK results show the ANFIS system achieves faster voltage stabilization and higher power (4.7kW) compared to the conventional P&O technique.

In (Karim, 2025) suggestion an optimization strategy integrating Direct Torque Control (DTC) for the induction motor with Particle Swarm Optimization (PSO) for MPPT in Photovoltaic Water Pumping Systems (PVWPS). This approach significantly reduces torque, power, and flux ripples, while improving system responsiveness and water output compared to an ANN-DTC system. The efficacy and dependability of the suggested PSO-based approach are validated in real time.

In (I. Saady et al., 2025) also proposed an ANN-based control approach that focuses on Direct Torque Control (DTC) for the induction motor as well as MPPT to improve Photovoltaic Water Pumping Systems (PVWPS). The proposed method replaces conventional MPPT and DTC components with ANNs, aiming to optimize PV power extraction and mitigate DTC's inherent issues like flux and torque ripples. Real-time simulations demonstrate significant reductions in ripples, improved response time, and increased water output, validating the efficacy of the ANN-based controllers.

In (Mesfin, 2025) offered a solar-powered water pumping system for off-grid Ethiopian farming that uses a BLDC motor and Zeta converter in conjunction with an ANN-based MPPT to solve the problem of food security. The system achieves 410W peak power and stable 2500

rpm motor speed, with the ANN-MPPT ensuring efficient, rapid stabilization (0.5s) under varying sunlight. This reliable, eco-friendly solution significantly improves water access in remote areas, enhancing agricultural productivity.

(R. D. Prasad and A. Hemasekhar) proposed an ANFIS-based controller to alleviate poor system response times and improve the efficiency of a Permanent Magnet Synchronous Motor (PMSM) drive powered by solar photo voltaic. It integrates an incremental conductance MPPT, an inverter, and an ANFIS-equipped Adaptive Hybrid Genetic Algorithm (AHGA) based Sliding Mode Controller (SMC) for speed regulation and harmonic reduction. The system's performance for irrigation applications is validated using MATLAB/Simulink.

In (P. B. Biragbara, 2022) focused on optimizing a 100 kW hybrid PV-wind turbine system using a Fuzzy Logic Controller (FLC) to manage charge/discharge and maximize power output. The FLC effectively minimizes oscillations and tracks the peak power point within 0.25 seconds, significantly improving output voltage, current, and overall system efficiency. Simulation results demonstrate a notable increase in voltage (from 824.13V to 903.249V) and efficiency (from 68.99% to 78.32%) after optimization.

In (S. Manna, 2023) suggested a new Robust Model Reference Adaptive Controller (LRMRAC) based on Lyapunov for effective Maximum Power Point Tracking (MPPT) in photovoltaic (PV) systems, especially when there are several power peaks due to partial shade. By outperforming both conventional and cutting-edge techniques (ANFIS, INC, VSPO, and P&O) across a range of load and weather scenarios, the LRMRAC seeks to quickly and precisely track the global MPP. Its higher performance, which achieves MPP and GMPP within milliseconds, is demonstrated by both simulation and OPAL-RT real-time results.

In (S. S. V Mohan, 2025) examined fault classification and optimized Maximum Power Point Tracking (MPPT) in solar photovoltaic (PV) systems, especially in partial shadowing situations (PSC). It evaluates nature-inspired algorithms (Dragonfly, Moth Flame, Grasshopper, and Slap Swarm Optimization) for MPPT, with the Slap Swarm Optimization Algorithm (SSOA) demonstrating the highest tracking efficiency of 98.38%. For fault classification, deep learning techniques including Random Forest, ANN, SVM, and CNN are explored, and the Convolutional Neural Network (CNN) achieves the maximum accuracy of 94.11%. The study

comes to the conclusion that the overall performance of solar PV systems can be greatly improved by combining these optimized MPPT and fault classification models.

In **(Ali ME, 2020)** paper Both central power plants linked to the electric grid and loads in remote locations have been fed by solar photovoltaic energy systems (PVES). Numerous studies have been conducted to lower the price of the energy produced by PVES. One of the most crucial aspects of research is lowering the cost of energy generation by increasing the amount of energy produced by the PVES through adjustments to its performance operations. This can be accomplished by monitoring the PV systems' maximum power output, which can significantly boost the energy produced by PVES and lower its cost. The maximum power point tracker (MPPT) is a device that monitors the maximum power available from the PVES. To ensure that it gets the most power possible from the PVES, MPPT employs a regulated method to regulate the power electronics converters. Traditional MPPT methods, such as hill climbing, incremental conductance, perturb and observe, etc., were first used a long time ago and were quite effective for un shaded PVES. The PV array's PV curve, however, produces many peaks under partial shade situations, which could trap traditional methods to fall inside one of the local peaks. Alright.

In **(Revathy, 2022)** Accordance to the report, the output power of solar modules is nonlinear with respect to the environmental circumstances. In order to optimize the solar photovoltaic system (SPVS), this work proposes a maximal power point tracker (MPPT) based on an adaptive neuro-fuzzy inference system (ANFIS). The output power of a DC-DC converter coupled to a 400 W PV array is optimized using the controller model. The technical data's major attributes are used to examine the complete model using MATLAB/SIMULINK. The controller model's behavior is evaluated under a range of weather and partial shade scenarios.

Research gaps: Limited studies apply ANFIS in solar water pumping with FOC control of PMSM motor.

- **Research contribution**: First-time modeling of ANFIS MPPT in PV-PMSM pumping system under Ethiopian site data, with a design-performance.

2.2 Theoretical backgrounds

2.2.1 Photovoltaic Energy System

Solar energy, which is produced at the sun's core by the fusion of hydrogen atoms into helium, is essential to life on Earth. A small fraction of this energy approximately two millionths reach our planet. This solar energy is transformed into electrical power using solar cells, which are composed of semiconductor materials and work via the photovoltaic effect.

These cells are organized into PV panels to achieve the desired voltage and current levels. To enhance energy extraction, power electronic converters serve as an interface between renewable energy sources and power systems, optimizing the conversion of solar energy into usable electrical power (A. Halmous, 2024). Figure 2.1 depicts the photovoltaic energy system.

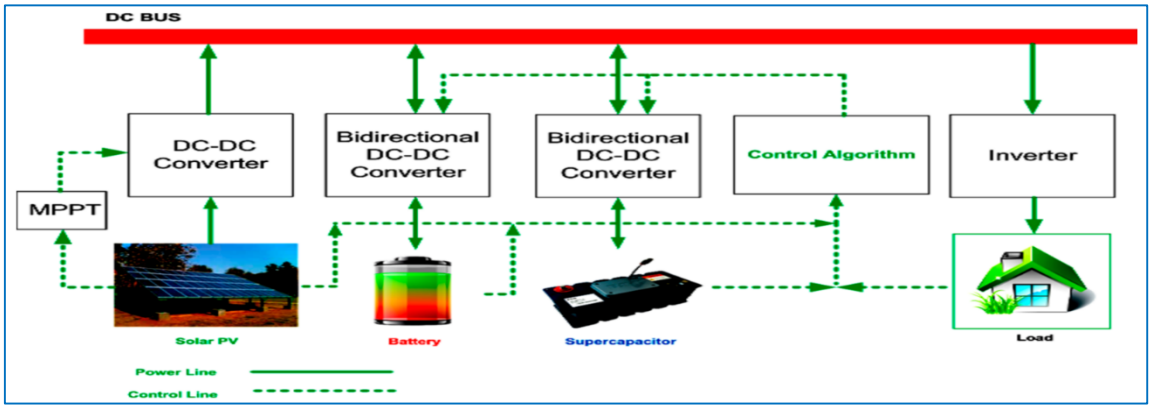

Figure 2. 1: Photovoltaic energy system

PV modules or arrays convert solar irradiation into electrical energy. A DC-DC converter modifies the voltage level to match the output voltage with the needs of connected electrical equipment. Depending on the required voltage, this converter can function as a buck, boost, or buck-boost converter. To get the most power out of the PV modules, the maximum power point tracking (MPPT) method is used. Through the use of a bi-directional converter that permits current flow in both directions, the system charges a battery when there is surplus power and uses the battery to discharge energy to the load during power outages (Ranjan, et al., 2021).

The simplest component of a photovoltaic system is a solar cell. Typically, a single PV cell can produce up to 1 or 2 watts of power. Each solar cell's semiconductor material creates a p-n junction, which is analogous to a diode The photovoltaic effect allows the connection to

generate currents when light is absorbed. A forward-biased diode is connected in parallel with the current source in Figure 2.2, which represents the equivalent circuit of a solar cell.

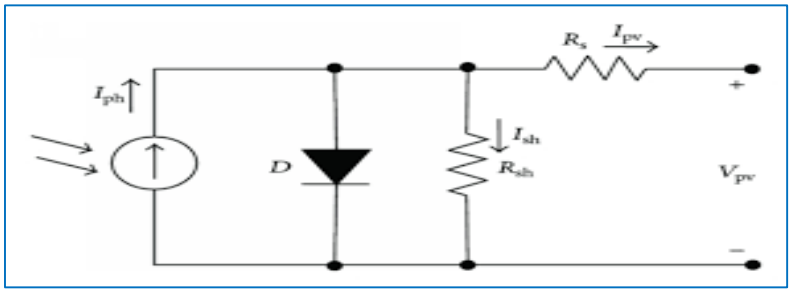

Figure 2. 2: Photovoltaic energy conversion system (Gursoy, M.; Zhuo, G.; Lozowski, A.G.; Wang, X, 2021)

The load is connected to the circuit's output terminals. The solar cell's current equation is provided by.

$$P = VI \qquad (2.1)$$

where I is the solar cell's current (A), V is its operating voltage, and P is its output power (W).

By merging to form larger units of modules, PV cells may generate more electricity. Modules can then be joined to create arrays, which are even bigger units. The entire power-generating system is a photovoltaic array, which is made up of any number of PV modules and panels (Magaji N. W., 2022).

2.2.2 PV cell

A photovoltaic cell, which is made of semiconductor materials like silicon and germanium, is the primary part of a solar system. Photovoltaic cells use silicon because of its advantages over germanium. When photons hit the surface of solar cells, covalent bonds within semiconductor atoms are broken and releasing electrons and holes. As a result, positive and negative terminals are generated, creating an electric field. Electric current will start flowing when a conductor connects these terminals (Al-Ezzi, 2022)

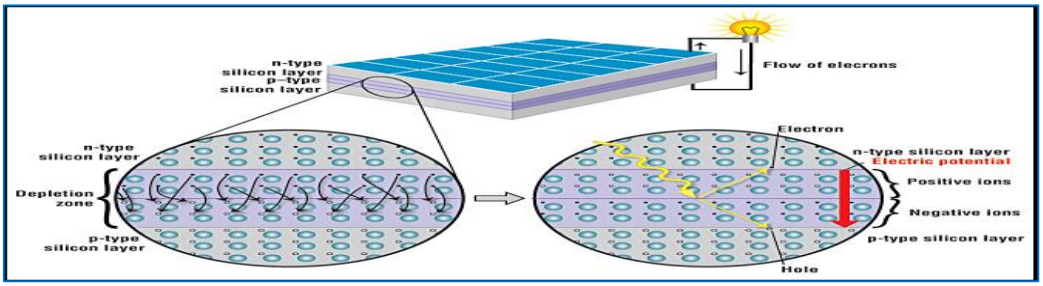

Figure 2.3: PV cells

2.2.3 Main PV cell types

Figure 2.3 shows the PV cells for silicon photovoltaic cells. Silicon is a material commonly used in the solar cell production process. Based on the structure of the raw material used to make them and the specific method of preparation, silicon photovoltaic cells are separated into four types (Elssaify, 2024)

- Solar cells made of single- or mono crystalline silicon.
- Solar cell made of poly/multi crystalline silicon.
- A thin-film, amorphous silicon solar cell.

Silicon solar cell with a string ribbon

Mono-crystalline PV Cells: are made from pure silicon single crystals that have been cut out from ingots. It is dark color and trimming around each of its corners set it apart easily from poly-crystalline panels. It works better if there is a need for low-energy sources. This technology has a great capacity for heat resistance and is the first generation of all PV cells. This technology's disadvantage is that manufacturing takes longer. The process for producing mono-crystalline silicon involves supersaturating high purity silicon first, then melting seed crystals into the molten silicon. In order to obtain silicon ingot, the seed crystal is then slowly extracted from the melted mono-crystal using the Czochralski mechanism. The crystal is also cut into smaller pieces to create cells, modules, and arrays. This technology can produce 140W of power from 1000W/m^2 of solar radiation on 1m^2 surface area of PV cells. Figure 2.4 shown as below depicts that the structure of monocrystalline PV cell.

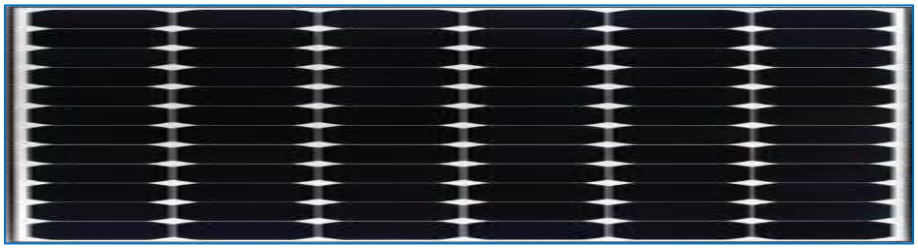

Figure 2.4: Monocrystalline PV cell

Polycrystalline PV Cells: It is made from several tiny pieces of silicon crystal block. They are currently considered to be the cells that are used the most. Due to the fact that these PV cells are not made from single crystals but rather from a combination of many crystals, they are less effective than single crystalline cells. When slightly shadowed, they perform mono-crystalline materials. With this method, 1000W/m^2 of solar energy can be converted to 130W of power over a 1m^2 surface area of PV cells. The production of this type of cell is more efficient than mono-crystalline. Molten silicon must be formed into blocks, which are subsequently separated into slabs, in order to create the crystals. Poly-crystalline solar panels must be larger to generate the same amount of watts because mono-crystalline solar panels are more efficient per square than multi-crystalline solar panels. Therefore, when comparing the two in terms of size to get a high-power output, single-crystalline PV panels are more beneficial. Additionally, the polycrystalline PV cell was shown in Figure 2.8.

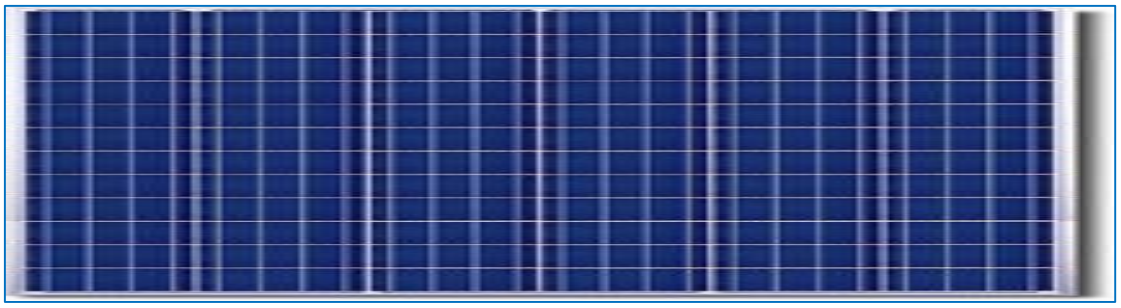

Figure 2.5: Polycrystalline PV cell

Thin-Film PV Cells: To use actual crystal, the silicon is deposited on glass, plastic, or stainless steel to form the solar module. Although the production costs are lower, these PV cells are much less efficient than the two types mentioned above. The inefficiency shows that large panels of this type have to generate the same amount of power as monocrystalline or

polycrystalline panels. Their lifespan is between 15 and 20 years, and their efficiency ranges from 5 to 13. Figure 2.6 presents the structure of Thin film PV cell as depicted in below.

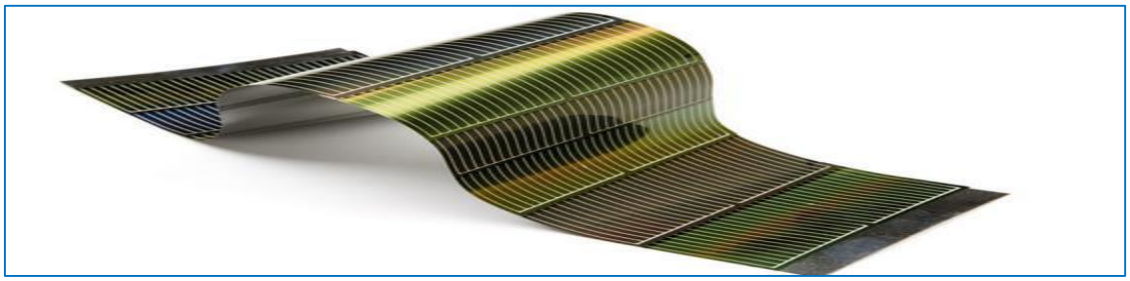

Figure 2.6: Thin film PV cell

String Ribbon Solar Cells: Production of polycrystalline silicon has been improved in this approach. Since it requires less labor to produce, the costs are even lower. Instead of using an ingot, ribbon-type photovoltaic cells are produced by developing a ribbon from the molten silicon. These cells function in the same way as mono crystalline and polycrystalline cells. Cell efficiency ranges between 8% and 10%. The efficiency of cells decreases as temperature increases. Compared to crystalline cells, thin-film cells are less susceptible to heat. A crystalline cell's production drops by about 0.5% for every degree Celsius as the cell's temperature rises. Since amorphous silicon cells' output reduces by about 0.2% for every degree Celsius more heat, they may be preferable in extremely hot conditions. As a result, modules should be maintained as cool as possible. Silicon poly crystals are used to make String Ribbon solar panels. Highly heat-resistant wires are used in their production. Thin silicon ribbons are produced when these wires are pulled through molten silicon. These solar panels are similar to conventional polycrystalline panels. The string ribbon solar cell also depicted in the following Figure 2.7.

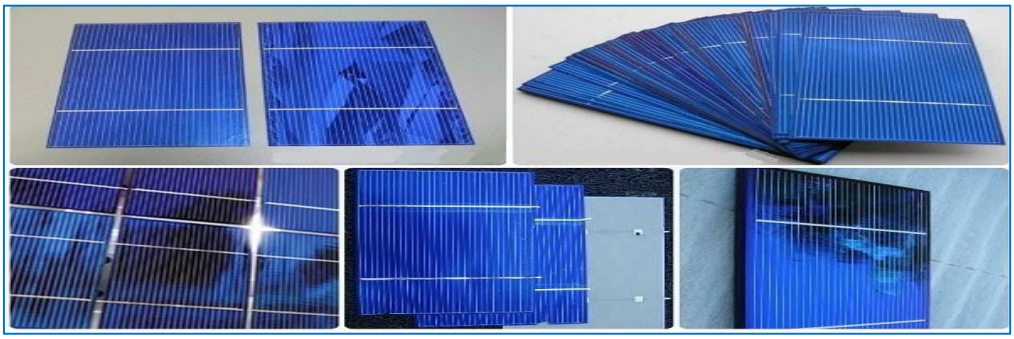

Figure 2.7: String ribbon solar cell

Mono or single-crystalline silicon is the focus of this work due to its effectiveness, space efficiency, and long life. Mono or single-crystalline silicon solar panels typically have an efficiency of 14 to 22%.

PV module

Silicon crystalline solar modules make up the great majority of solar modules now on the market for use in residential and commercial solar systems. These modules are installed inside an aluminum frame and are made up of several strings of solar cells connected in series (positive to negative). A total of 0.5 volts may be generated by each solar cell. The maximum output of a 36-cell module is 18 volts. Larger modules will have a frame with 60 or 72 cells. The amount of amperage a cell contains is determined by its size or surface area. The amperage increases with cell size.

PV panel

A solar panel, also called a photovoltaic module, is a collection of solar cells arranged in a framework for installation. Solar cells use sunlight as its energy source to produce direct current electricity. PV arrays are groups of PV panels, whereas PV panels are groups of PV modules.

PV Array

Simply said, a photovoltaic array is a group of PV modules connected in parallel and series. The modules are connected in a grid or array to meet the load demand because the electricity generated by individual modules would not be enough to meet the load requirement of trading applications. The connections between modules in an array are comparable to those between cells in a module. When constructing a photovoltaic array, the modules are frequently connected in parallel to supply additional current when needed, and then serially to achieve the appropriate voltage. Figure 2.8 shows the PV arrays together with their creation order.

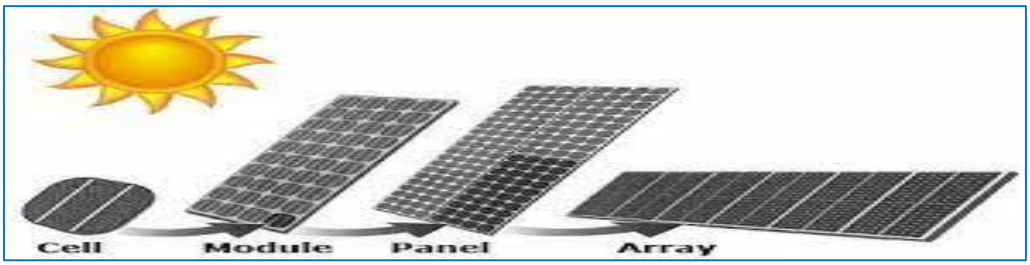

Figure 2.8: PV array

2.2.4 Three elements influencing the performance of photovoltaic modules

Load Resistance: The voltage at which the module operates will be determined by a load or battery. For instance, the battery voltage in a nominal 12-volt system is often in the range of 11.5 to 14 volts. The modules must run at a little greater voltage than the battery in order for the battery to charge. The module will function at or close to the maximum power point, yielding the highest efficiency, if the resistance of a load is properly matched with the I-V curve of the module. The efficiency of the solar module declines as the load resistance rises, forcing the module to run at a voltage above its maximum power point. At voltages lower than the maximum power point, efficiency likewise declines.

Intensity of Sunlight: The amount of solar radiation that a photovoltaic module is exposed to has a proportionate impact on its production. Module output will increase with stronger sunshine. Lower current output is the effect of less sunshine. Variations in the intensity of the sun do not significantly alter voltage.

Cell Temperature: Higher cell temperatures result in less efficient operation of photovoltaic modules. As the cell temperature rises, the operational voltage decreases. In this instance, heat can be viewed as an electrical barrier that prevents electrons from moving freely. If a module's or array's maximum power point moves to a voltage that is substantially lower than the load's operating voltage, the effective current output could be drastically diminished

Shading: The output of solar modules will be drastically reduced even if they are partially shaded. The output of this module can be lowered by up to 80% in a single fully shaded cell. When running at 15 volts, the output of the module is reduced by half due to the partial shading of three cells. The impacts of reduced insolation effects and cell temperature are displayed in Figure 2.12.

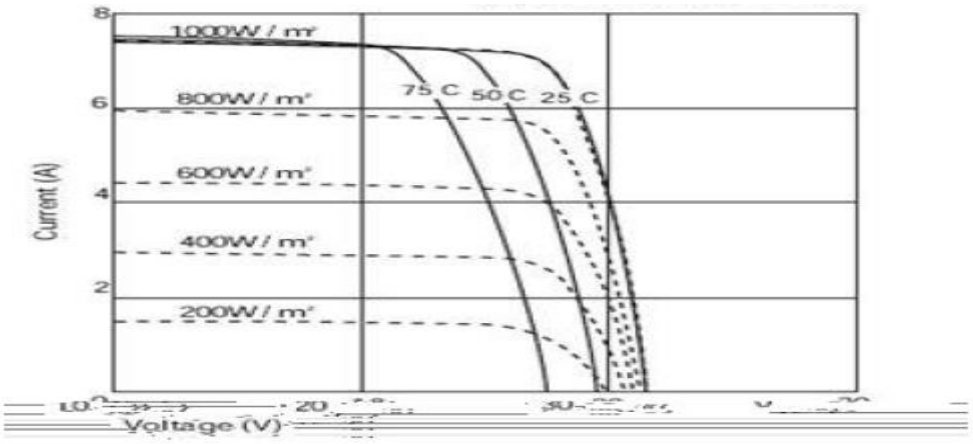

Figure 2.9 Effects of Cell Temperature and Reduced Insolation Effect

2.2.5 Maximum power point tracking (MPPT)

There are benefits and drawbacks to each of the numerous Maximum Power Point Tracking (MPPT) systems that have been created. While traditional methods such as Incremental Conductance (INC) and Perturb and Observe (P&O) are praised for their ease of use and simplicity, they typically generate oscillations around the MPP, which invariably results in power losses. However, more advanced MPPT techniques that make use of artificial intelligence (AI), like Adaptive Neural Fuzzy Inference System (ANFIS), Fuzzy Logic Controllers (FLC), and Particle Swarm Optimization (PSO), produce better results, especially in difficult variable scenarios like partial shading or abrupt environmental changes.

Induction motors (IMs) are frequently employed in PV-powered water pumping systems due to their economic viability, dependability, and operational efficiency. Nevertheless, their inherent nonlinear characteristics pose a challenge to effective control. Simpler Scalar Control (SC) methods are straightforward but yield insufficient torque response at lower frequencies. While more advanced techniques like Indirect Field-Oriented Control (IFOC) provide superior control over torque and speed, their effectiveness is reliant on accurate motor parameters. To achieve optimal performance, characterized by quicker response, improved dynamics, and reduced reliance on precise motor parameters, Direct Torque Control (DTC) has been introduced (Karim, I. Saady and M., 2025).

2.3 DC to DC Converters

Electronic circuits known as DC-DC converters are vital components of contemporary power management systems. In order to provide steady and effective power supply to a variety of electronic devices and systems, their main job is to change the voltage of a direct current (DC) source from one level to another.

A DC-DC converter is a power electrical circuit that converts a DC voltage between different voltage levels. There are various conversion methods, such as switched-mode, electrical, magnetic, linear, and capacitive. Among these are switched-mode DC-DC converters, which are the circuits described in this thesis. This gadget is used to switch direct current electrical power between different voltage levels when necessary. DC-DC converters are especially important since DC cannot be easily ramped down or up using a transformer. Thus, a transformer is created using a DC-DC converter. Essentially, they do is transform the supplied power into different impedance levels (DC to DC converter pdf,, [Accessed 11, 02, 2023].) Consequently, electricity is generated from the input independent of the output voltage levels. There are various kinds of DC-DC converters that can be used to change the voltage level. Below is a discussion of a few of them.

The buck converter: Depending on its needs, the buck converter is employed in circuits to step down the voltage level from the input voltage. Buck converter is easy and inexpensive. When a buck converter is operating, the switch is initially open, which means that no current is flowing through any section of the circuit. When the switch is closed, however, a gradual buildup of current begins to flow through the inductor. Because the inductor draws current through the diode, the voltage at the inductor's output is lower than the initial value when the switch is closed.

Boost Convertor: A boost converter, also known as a step-up converter, is a power converter that produces a greater DC voltage output than its input DC voltage. Where power conservation is required, the source current exceeds the output current. The components of this converter are identical to those of a buck converter, however the output voltage is greater than the source voltage.

Buck-Boost Converter: Buck-boost converters are another common type of switched-mode converter. This buck-boost converter will either have a higher or lower output voltage than the input voltage.

2.4 Inverters

Any standalone PV system with ac loads needs inverters, also referred to as power conditioning equipment. The system's DC operating voltage will be affected by the inverter that is utilized. Both the DC input and the AC output requirements must be taken into account when designing an inverter. The range of voltage, frequency, and waveform fluctuations that can be tolerated should be taken into account while building the AC load, in addition to the inverter's power requirements.

The DC voltage, surge capacity, and allowed voltage variation of the input side must be specified. Before choosing the ideal inverter for a certain application, a number of factors must be carefully taken into account. The choice of inverter will affect the performance and reliability of a PV system.

2.4.1 Types of Inverters

Systems with adjustable AC drives typically use one of two main types of inverters. Voltage source inverters and current source inverters are the names given to them, respectively. After receiving DC power from a source with a variable voltage, the variable voltage inverter (VVI), also known as the square-wave six-step voltage source inverter (VSI), modifies the frequency and voltage. An adjustable current source provides DC power to the current source inverter (CSI), which modifies the frequency and current.

CHAPTER 3
METHODOLOGY

3.1 Resource Potential Assessment of solar Energy

Ethiopia as a whole has an average daily radiation of 5.26 kWh/m2. This varies significantly throughout the year, ranging from a minimum of 4.55kWh/m2 in July to a maximum of 5.55kWh/m2 in February and March (Mekonnen, 2024)**.** The yearly mean radiation levels in the Itang region of the Gambella Regional State (Western Ethiopia) range from as low as 4.25 kWh/m2 to as high as 6.25 kWh/m2 in the Adigrat region of the Tigray Regional State (Northern Ethiopia). In contrast to diffused sunlight, which is scattered by dust, humidity, pollution, and other factors, direct solar energy travels straight to the earth's surface.

"Global-horizontal isolation" describes the overall amount of sunlight, including direct and diffuse. Sunlight hour and solar radiance are the two primary factors that determine the efficiency of solar power plants. The first element is a climatological indicator, which calculates how much sunshine a certain location on Earth receives during a given time period. Usually, an average value over a period of years is used to express it.

Five to six hours a day are commonly referred to as the sunshine hour. The second factor is solar irradiance, which is the power per unit area that is obtained from the sun in the form of electromagnetic radiation within the wavelength range of the measuring apparatus. The Ethiopian National Metrology Agency has reported the sunshine hour in the Oromia region's Dodota woreda.

3.1.1 Site selection

Although many designers tend to undervalue site selection when sizing PV water pumping systems, it is essential for a sustainable water supply plan. The kind and quality of the water supply, along with the quantity of water needed for the planned use, are the primary factors in site selection. The Arsi zone of Ethiopia's Oromia region dodota woreda, which is closest to Lake Ziway, was selected for the study.

Figure 3. 1: Amude, Arsi zone, Ethiopia Source: Google map

Amude is located in Ethiopia's Oromia Regional State, as shown in Figure 3.1 of the Google Map. It is a waste of money to install the best system without a dependable water supply. Similarly, if a system is designed without taking into account the actual demand for water, it could result in inadequate water supply or needless expenses for an overly large system. The amount of water needed is taken into consideration when constructing a solar water pump system. This irrigation technique requires knowing the crop's average water requirements on the property. When putting this system into place, one must be more precise because this requirement differs depending on the location. As a result, the chosen site area is 1000,000 m2, or nearly 1000m x 1000m. The flow rate of the water can be computed. The irrigation water application depth (ET rate) must be considered in order to calculate the irrigation water flow rate. For the purposes of this study, maize is considered the primary crop in the area, and its ET rate is 0.005 m/hr (Aklilu, june 2023).

The ET rate (m/hr) multiplied by the site's area (m2) yields the amount of water needed per hour for the specified crop area. Consequently, 5000 cubic meters per hour (m^3/hr) or 5000,000 L/hr of water flow rate is needed to irrigate a 1000,000 square meter maize crop at an ET rate of 5 mm/hr.

3.1.2 Water Source

The next major objectives are to locate the water source and take it into account. Rainfall, groundwater, or surface water could be its source. The river, pond, spring, borehole, and well are common sources. One must examine the source's static and dynamic water labels in order to determine the source of the water. The gap between the well's top and the water's surface is level and static. Seasonal changes may be occurring.

The dynamic level, as opposed to the static level, is the difference between the well's top and the water's surface when the pump is running. It can be measured because it typically decreases when the pump is running. To make sure that the dynamic water level stays consistent throughout the year, some testing or observation is necessary because the amount of water may change depending on the season.

Step1. Determining Flow Rate for Pump

The pump's flow rate is assessed by taking into account the peak hours of the sun and the monthly water use. The month with the least amount of insolation has been chosen to ensure that the system is not undersized for any given month of the year. By dividing the expected daily water amount by the number of peak sun hours per day, the pump's flow rate is analyzed. The average solar hour per day is 5.47, according to Table 3.2. Equation (3.1) can be used to compute the pump flow rate design.

$$flow\ rate = \frac{(daily\ water\ requirement)}{(peak{-}sun\ hours)} \tag{3.1}$$

$$flow\ rate = \frac{5000000\ {}^{L}/_{Hr}}{5.47\ peak\ sun\ hour * 60\ {}^{min}/_{hr}} = 15{,}234.6\ {}^{L}/_{min}$$

Step 2. Determine dynamic Friction-induced loss of head and head

The overall lifting height is the main variable in a solar-powered water pumping system. This is because the force needed to move the water from the deep level of the well to the desired level must be calculated.

$$T_h = f_h + D_h + H_{pipe} + P_h + V_{Rh} + V_h \tag{3.2}$$

Equation (3.3) uses the Darcy-Welsbach formula to compute the head due to friction loss fh.

$$f_h = \frac{fLV^2}{2*d*g} \tag{3.3}$$

where d is the pipe's diameter, g is gravity, L is the pipe's length, C is the fluid's mean velocity, and f is the friction factor. But determining the friction component is too difficult or complicated. The Blasius equation can be applied to smooth pipes and flow (Renewable energy, Design guide and catalog, Shewin Electric, , 2008-2009.)

$$f = \frac{1.325}{\left[\ln\left(\frac{e}{3.7d} + \frac{5.74}{R_e^{0.9}}\right)\right]^2} \quad (3.4)$$

Reynolds' coefficient Re is obtained as

$$R_e = \frac{\rho v d}{\mu} \quad (3.5)$$

The formula for calculating a fluid's average velocity, V, is

$$V = \frac{Q}{A}$$

Where Q is discharge rate, A is the pipe's area and V is fluid's average velocity and it is determined by

$$V = \frac{4*Q}{\pi*d^2} \quad (3.6)$$

Then, it can be calculated as,

$$v = \frac{4x0.0037}{\pi * 0.05\text{^}2}$$

$$= \mathbf{1.917\ m/sec}$$

Now that the Reynolds value has been calculated using Equation (3.4),

$$R_e = \frac{\rho v d}{\mu} = \frac{1000\ {}^{kg}/_{m^3} * 1.91\ {}^{m}/_{sec} * 0.05m}{1.14 * 10^{-3}\ {}^{Ns}/_{m^2}} = 84{,}078$$

Re is the Reynolds number, μ is the dynamic viscosity (1.14*10-3 Ns/m2), and ρ is the water density (1000 kg/m3). The type of flow depends on the value of Re ("Engineering ToolBox. Hydraulic Diameter, 2019.).

- The flow is referred to as laminar if Re is less than 2000.
- The flow is referred to as turbulent if Re is more than 4000.
- 2000 < Re < 4000 indicates a transitional flow.
- The flow in this system is turbulent because Re >4000.

Materials	Roughness(ft)
Asphalted cast iron	0.0048
Commercial steel	0.0018
Drawn bass or copper	0.00006
Galvanized iron	0.006

PVC pipe	0.0000015
Wrought iron	0.0018

Table 3. 1: Common pipe materials

For PVC, the relative roughness is: ε ≈1.5*10^{-6} m,

$$\gamma = \frac{\varepsilon}{d} = \frac{1.5*10^{-6}}{0.05} = 3 * 10^{-5} \quad (3.7)$$

Since, R_e > 4000, applying the above Equation (3.4) the friction factor is determined as shown below.

$$f = \frac{1.325}{\left[\ln\left(\frac{e}{3.7d} + \frac{5.74}{R_e{}^{0.9}}\right)\right]^2} = 0.1844$$

Consequently, the head loss resulting from friction fh is calculated using Equation (3.3) as follows:

$$f_h = \frac{fLV^2}{2 * d * g} = \frac{0.184 * 100 * 1.9^2}{2 * 0.05 * 9.81} = 11.4m$$

Step3. Determine how much Total Dynamic Head (TDH) is needed to pump the water.

The dynamic head loss can be found using the Darcy-Welsbach equation as follows:

$$D_h = K\frac{V^2}{2*g} \quad (3.8)$$

Where: K is the combinations of the pipe (straight length) and fittings (bends) gain values.

$$K = K_{pipe} + K_{fitting} \quad (3.9)$$

K_{pipe} is linked to the system's pipe's straight length, which is defined as:

$$\boldsymbol{K_{pipe} = \frac{fL}{d} = \frac{0.184*100}{0.05} = 40} \quad (3.10)$$

$K_{fitting}$ is the term used to describe the fittings used in the conduit that moves water from the receiving tank to the surface. The individual fitting values from the standard tables can be added to determine the total $K_{fitting}$ values. The $K_{fitting}$ calculation for the system in question is shown in Table 3.2 below.

Items That Fit	The quantity of items	$K_{fitting}$ Value	Total
45^0 flanged	2	0.2	0.4
90^0 bends	3	0.75	2.25
No return valves	1	1	1
Valves (completely open)	1	0.3	0.3
Total $K_{fitting}$			**3.95**

Table 3. 2:Fitting consideration

Therefore, $k = K_{pipe} + K_{fitting} = 3.95 + 40 = 45.95 \cong 44$ So, referring Equation (3.9) D_h can be calculated as

$$D_h = 44 * \frac{1.9^2}{2*9.81} = 8.095\text{m}$$

The following formula can be used to determine the velocity head loss:

$$V_h = \frac{V^2}{2 * G} = \frac{1.9^2}{2 * 9.81} = 0.18$$

The horizontal pipe length H_{pipe}, vertical rise head V_{RH} and pump level head P_h are all regarded as being 8 m, 25 m, and 10 m, respectively. Thus, the total system dynamic head is ascertained using Equation (3.2) as follows:

$$T_{DH} = F_h + D_h + c + P_h + V_{RH} + V_{h=11.4+8.095+8+25+10+0.18=63m}$$

Step 4. Analysis of Power Requirement and pump size

The next step is to figure out how much power each part of the proposed system needs. Determining the power needed to get the water to the surface is a crucial first step. PV array, pump, induction motor, and other equipment dimensions are included. The needed hydraulic power P_h of the pump is determined as the first step of the power system analysis and is given by.

$$P_h = \frac{\rho q g T_{Dh}}{3600*1000} \quad (3.11)$$

Where:

P-power (kW)

ρ - is supply water density (1000kg/m^3)

g- Acceleration due to gravity

q- Flow rate of the water (L/s)

TDH- Total Dynamic Head (m).

Consequently, the water flow rate q can be computed as follows: where Q_{fr} is the water flow rate and P_{oh} is the pump operating hours. The mechanism is thought to operate for eight hours each day.

$$q = \frac{Q_{fr}}{P_{oh}} = \frac{5000\frac{m^3}{day}}{8\frac{hr}{day}} = 625\ \frac{m^3}{hr} \quad (3.12)$$

Thus, by using Equation (3.12), the hydraulic power of the pump is determined as follows:

$$P_h = \frac{625 * 1000 * 9.81 * 63}{3600 * 1000} = 107.29\ KW$$

The suggested range, assuming η=0.65, is 65 to 70 percent if the pump's efficiency is unknown.

$$P = \frac{P_h}{\eta} = \frac{107.29}{0.65} = 165.07\ KW \quad (3.13)$$

As mentioned in the earlier chapters, permanent magnet synchronous motor is taken into consideration for pumping the required amount of water. Its load power is provided by the following equation (3.14). pump motor efficiency of 0.7 is anticipated.

$$P_m = \frac{P}{\eta} = \frac{165.07}{0.7} = 237.81\ KW \quad (3.14)$$

Average temperature of the selected case study area

Table 3. 3: The research area's average monthly temperature

Month	Jan	Feb	Mar	Apr	May	Jun	Jul	Aug	Sep	Oct	Nov	Dec
^{0}C	28.9	29.6	27.4	29.1	29.2	27.6	21.9	20.2	24.9	25.3	25	24.6

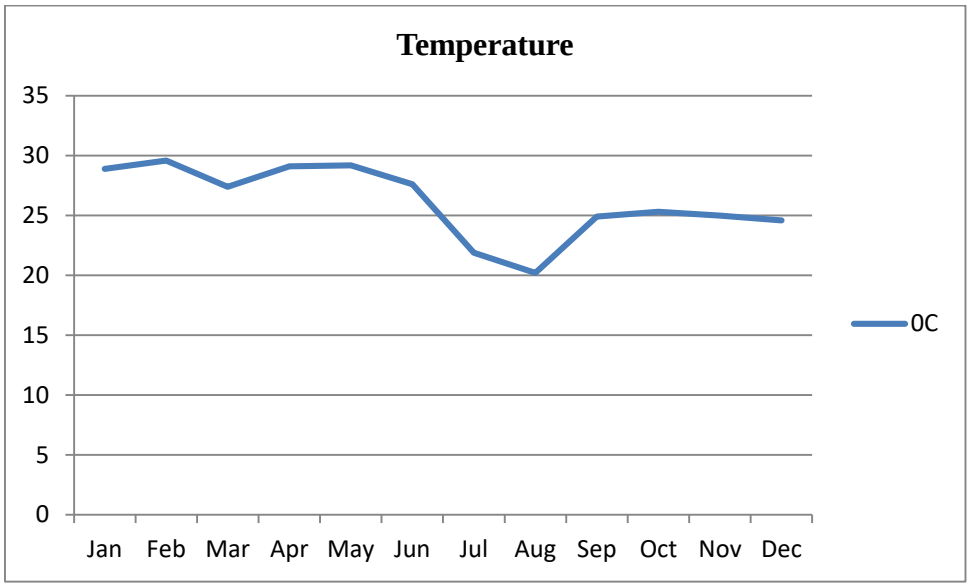

Figure 3. 2: Temperature profile obtained from site

This is followed by the estimation of the case study's solar insolation using the Angstrom-Prescott (A-P) model (U. Joshi, 22 June 2022).

$$H_o = \frac{24}{\pi} G_{SC} \left(1 + \cos \frac{360 n_d}{365}\right) * \left(\cos \varphi \cos \delta \sin w_s + \frac{\pi w_s}{180^0} \sin \varphi \sin \delta\right)$$

Where $\delta = 23.45^0 \sin (360^0((284 + n_d)/365))$,

$$\cos w_s = -\tan \varphi \tan \delta, H = H_0 \left(a + \left(\frac{bn}{N}\right)\right),$$

In which location, G_SC Is the solar constant (1.367kW/m2), φ is the latitude in degrees, δ is the solar declination in degrees, ωs is the sunset hour angle in degrees, and January 1st is taken as the first day of the year. N is the monthly average of the maximum hours of sunshine that can occur, n is the monthly average of the daily hours of sunshine, H0 is the monthly average of the daily extraterrestrial solar radiation, H is the monthly average of the daily global solar radiation, and a and b are empirical coefficients.

Table 3.4 calculates and illustrates the solar radiation using the aforementioned connection. The estimated range of the obtained solar irradiation is 5–7 kWh/m2/day. Compared to wealthy nations like Germany that use more renewable energy resources, the case study area's solar

insolation data shows that it has a lot of untapped potential resources for solar power plants. The annual average of the case study area's solar irradiance or insolation (kWh/m2/day) is displayed in Table 3.4 below.

Table 3. 4: Monthly average solar radiation of the study area

Month	Average (kWh/m^2)
Jan	5.86
Feb	6.20
Mar	5.69
Apr	6.04
May	6.11
Jun	5.18
Jul	5.14
Aug	5.28
Sep	5.62
Oct	5.28
Nov	5.68
Dec	5.45

3.1.3 Solar PV panel designing and modeling

For the PV to power the induction motor, careful planning is required. It is believed that the mechanism runs for eight hours every day. Pump power and operating hours are used to compute E_{use} daily energy consumption.

$$E_{use} = P_m * hours = 238kW * 8\,{}^{h}/_{day} = 1904\ {}^{kWh}/_{day} \quad (3.15)$$

The solar array must be sized to supply the 238 kW of power needed by the pump at the inverter output while taking all losses into consideration. System efficiency is caused by dirt, wiring, and inverters. For such systems, an average overall efficiency factor is 85% (0.85).

Step 1: needing the array's DC power

$$P_{array\ dc} = {}^{P_{load}}\Big/_{\eta_{sys}} = \ {}^{238\ kw}\Big/_{0.85} = 280\ KW \quad (3.16)$$

The overall system design is a 280 KW PV array and a 238 KW motor. Therefore, the irrigation system is designed to support commercial farming at the selected location.

Step 2: the quantity of PV modules needed

$$N_{module} = \frac{P_{Array\ dc}}{P_{mp}} = \frac{280\ 000\ W}{550\ W} = \approx 510\ Modules \quad (3.17)$$

Step 3: Configuring the PV array (parallel and series)

The number of PV modules connected in series (Ns) is determined using equation (3.18). For a 236 kW system, we must select a DC system voltage; 1000V is a typical DC input voltage for an inverter. Let's aim for an 800V V_{mp} .

$$N_s = \frac{V_{dc}\ target}{V_{mp}} = \frac{800\ V}{41.2\ V} = 19.42\ \approx 19\ Modules \quad (3.18)$$

Equation (3.20) is used to calculate the number of string in parallel (Np):

$$N_p = \frac{N_{module}}{N_s} = \frac{510}{19} = 26.57\ \approx 27\ Parallel\ string \quad (3.19)$$

The total number of modules in the PV array for the Advance power Hellene 96M475 PV type is then determined using equation (3.20), as shown below:

$$N_T = N_P * N_S = 27 * 19\ = 513\ \ modules \quad (3.20)$$

Final total module = 19 * 27 = 513
513 * 550 W = 282.15 KW is the final array power, which satisfies our 280 kw requirement.
Let's examine the module's available space.
Area for the 510 module is equal to 510 * 2.585 m² = 1.318 m².
Consequently, the area needed is less than 0.1% of the entire area that is available. Land is not a limitation.

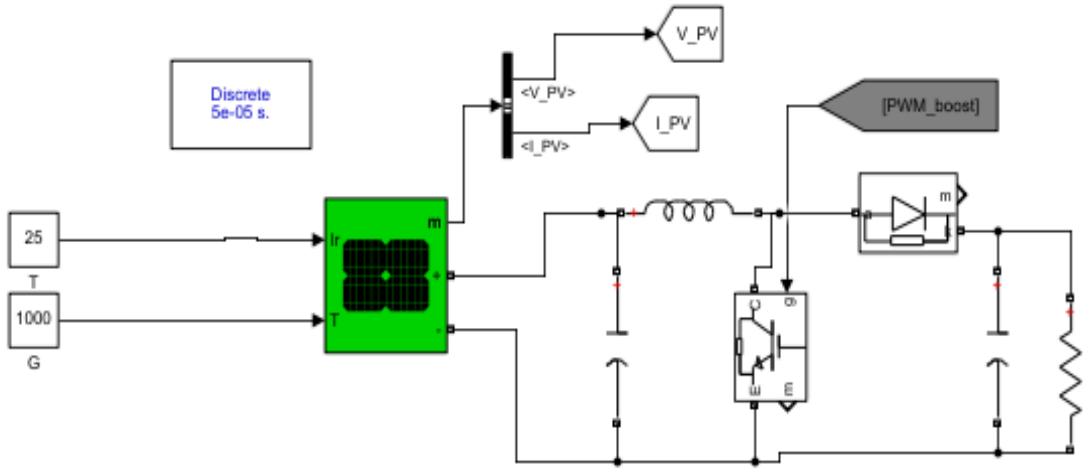

Figure 3. 3: Modeling of PV array with boost converter

The PV array connects multiple solar panels in series and parallel to convert sunlight into electrical energy. The PV array's output voltage is controlled and increased via a DC-DC converter known as a boost converter. A solar cell, often known as a "photovoltaic" (PV) cell, is a device that converts solar radiation into electrical power. A solar array can be created by joining several modules, each of which is made up of photovoltaic cells. The PV array consists of several modules coupled in series or parallel topologies. Depending on the fluctuating levels of irradiation during the day, the array's output may change significantly. PV cells make up the great bulk of the many PV modules that are connected in parallel and series to create photovoltaic arrays.

PV modules or arrays convert solar radiation into electrical energy. To adapt the output voltage to the requirements of connected electrical equipment, a DC-DC converter adjusts the voltage level. This converter can operate as a buck, boost, or buck-boost converter, depending on the voltage that is needed. The maximum power point tracking (MPPT) technique is used to maximize the power output of the PV modules. The system charges a battery during periods of excess electricity and uses the battery to discharge energy to the load during power outages by means of a bi-directional converter that allows current to flow in both ways (Ranjan, et al., 2021).

A solar cell is the most basic part of a photovoltaic system. One PV cell may typically generate up to one or two watts of power. The semiconductor material used in each solar cell forms a p-n junction, which is comparable to a diode. When light is absorbed, the connection can produce currents thanks to the photovoltaic effect. The equivalent circuit of a solar cell is shown in Figure 2.2, where a forward-biased diode is connected in parallel with the current source.

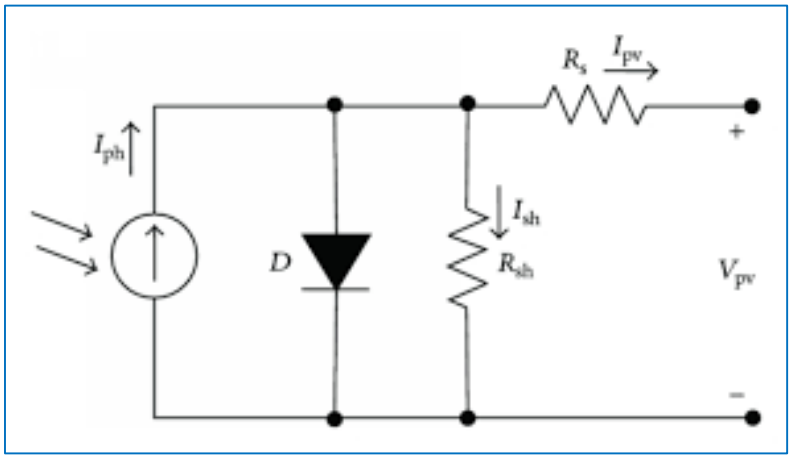

Figure 3. 4: Equivalent Circuit Model of a Solar Cell (Reddy K. H., 2020)

The load is connected to the circuit's output terminals. The solar cell's current equation is provided by.

$$P = VI \tag{3.21}$$

where I is the solar cell's current (A), V is its operating voltage, and P is its output power (W).

By merging to form larger units of modules, PV cells may generate more electricity. Modules can then be joined to create arrays, which are even bigger units. The entire power-generating system is a photovoltaic array, which is made up of any number of PV modules and panels (Magaji N. W., 2022).

To obtain the required current, voltage, and high power, the PV array is composed of several solar cells connected in series or parallel. Thus, PV systems can be built to accommodate almost any size or type of electrical requirement. Many PV systems have been running continuously outside on Earth or in space for more than 30 years. Below are the detailed input parameters needed to model a solar photovoltaic cell.

Step1:$I_{ph} = [I_{sc} + K_i(T - 298)] * {}^{I_r}/_{1000}$ (3.22)

where Iph is equal to photocurrent (A).

Short circuit current (A) is equal to I_{sc}.

Ki is the cell's short circuit current at 25°C and 1000 w/m^2.

T = temperature (K)

Ir = w/m^2 solar irradiation

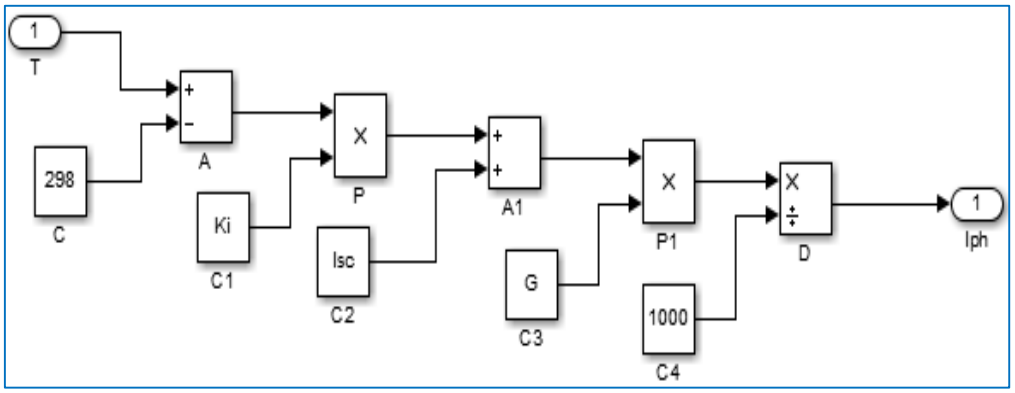

Step2: $\text{Ish} = \frac{\text{V}*\frac{\text{Np}}{\text{Ns}}+I*Rs}{\text{Rsh}}$ (3.23)

$$\text{Vt} = \frac{\text{k} * T}{\text{q}}$$

Where, Vt is the diode terminal voltage (V); Rs is the series resistance; Rsh is the shunt resistance; Ish is the current flowing through the shunt resistor; and Np is the number of PV modules linked in parallel.

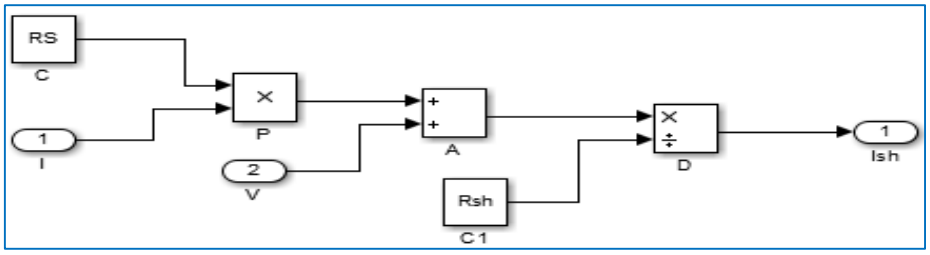

Figure 3.4: Expanded view of reverse saturation current mode

Step3: $\text{Irs} = \frac{\text{Isc}}{[\exp(\frac{qVoc}{NsknT})-1}$ (3.24)

As shown in Figure 2.3 the expanded view of reverse saturation current mode is presented.

Where, Irs = reverse saturation current

q = electron charge, = 1.6*10^{-19c}

Voc = open circuit voltage

Ns = number of cells connected in series

n = the identity factor of the diode

K = Boltzmann's constant = 1.3805*$10^{-23J/K}$

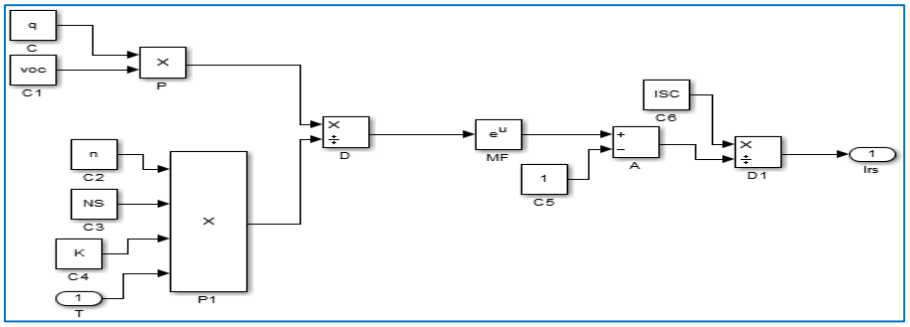

Step4: Io = $Irs\left[\frac{\mathrm{T}}{Tr}\right]^{3}\exp\left[\frac{\mathrm{q}*\mathrm{Ego}}{\mathrm{nk}}*\left[\frac{1}{T}-\frac{1}{Tr}\right]\right]$ (3.25)

Where, Io = saturation current

Tr = nominal temperature = 298.15K

Ego = band gap energy of the semiconductor, =1.1eV.

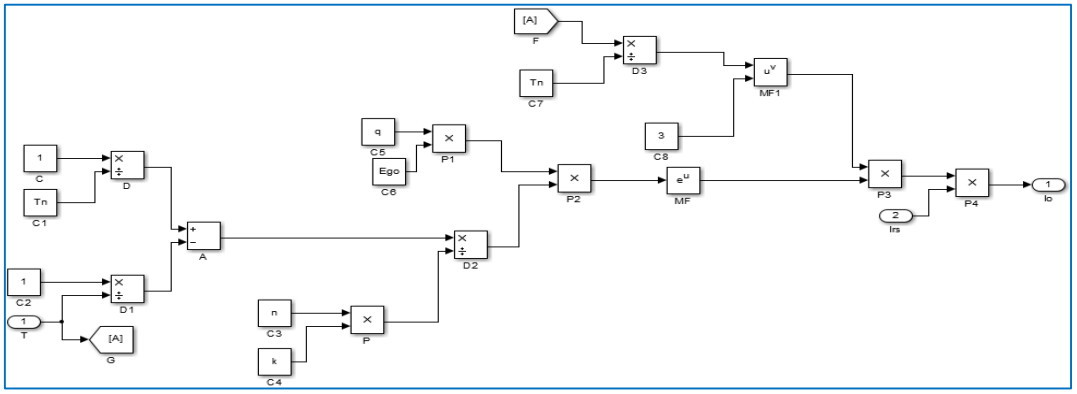

Step5: I = $Np \times Iph - Np * Io * \left[\exp * \left(\frac{\frac{\mathrm{V}}{\mathrm{Ns}}+\mathrm{I}*\frac{\mathrm{Rs}}{\mathrm{Np}}}{n*Vt}\right) - 1\right] - Ish$ (3.26)

Where, I = output current

These is very important equation since which is coming from the equivalent circuit.

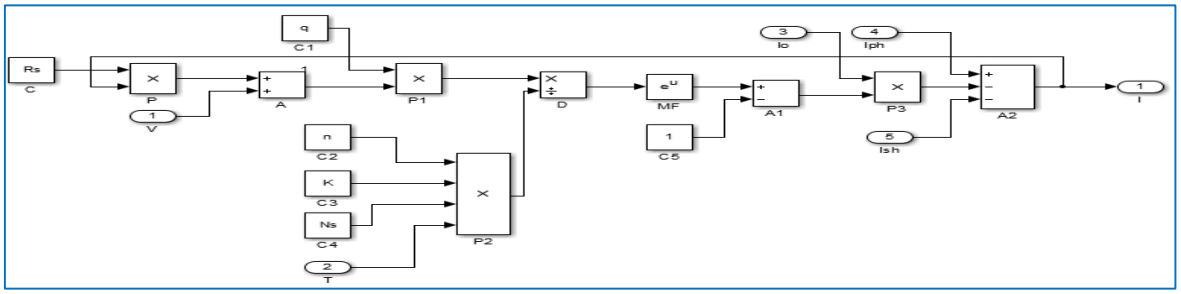

Simulink modelling of PV module

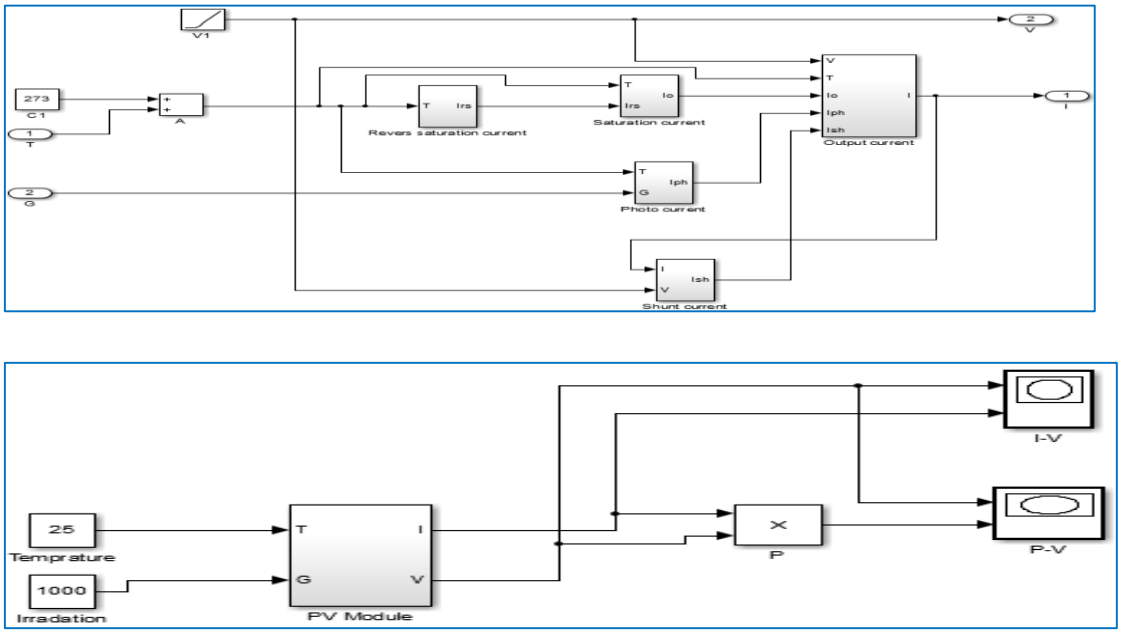

Figure 3.5: PV module Simulink modeling

Here, Figure 3.5 discusses PV module modeling, and Figure 3.6 below illustrates the outcome. The I-V and P-V curves of the PV module are displayed when the circuit model is simulated using Mat lab Simulink program.

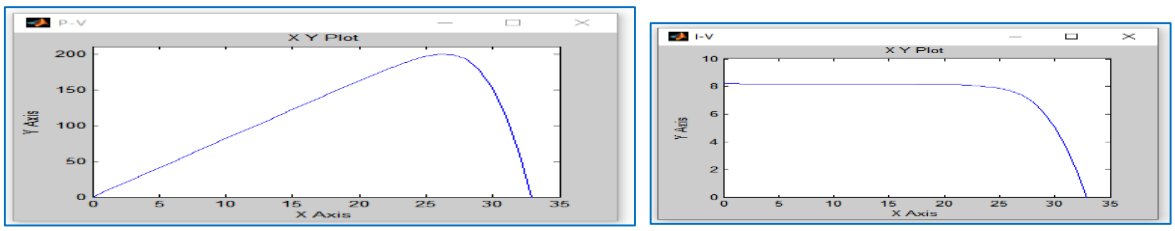

Figure 3.6: Power -voltage (PV) and Voltage-current (VI) characteristics of solar cell

Table 3. 5: Specification of Hellene 96M475 PV Array

Parameters	values
Open-circuit voltage (Voc)	62.39 V
Short-circuit current (Isc)	13.7 A
The voltage at Pmax (Vmp)	41.2V
Current at Pmax (Imp)	13.35A
Voltage temperature coefficient β (Voc)	-0.31 %/ ^{0}C
Current temperature coefficient α (Isc)	0.055 %/ ^{0}C
Peak Power (Pmax)	550 W

where Vtn is the nominal voltage, Vd is the voltage across the diode, and Vocn is the open circuit current. T is the operational temperature of the module in Kelvin, while ΔT is the Kelvin variation from the nominal temperature. The diode saturation current is denoted by Id. G is the actual irradiance in W/m2, IPV is the photovoltaic cell's light-generated current, and Gn is the irradiance under normal conditions.

Additionally, G0 is the nominal irradiance, or 1000 W/m2, and G is the sun irradiation (W/m2). The module short-circuit current is measured under standard test conditions (T = 25°C and G = 1000 W/m2) using data from the reference model. NS and NP are the number of cells linked in series and parallel, respectively; Ir,sat is the reverse saturation current of the module; q is the charge of an electron; Voc (VPV) is the open-circuit voltage of the module; and Eg is the bandgap energy of the semiconductor. The analogous series and parallel resistances of the module are denoted by the letters RS and RP, respectively.

The photovoltaic current and voltage at the maximum power point are referred to as maximum power point current and maximum power point voltage, respectively. Maximum power point current and voltage are denoted by the acronyms Imp and Vmpp, respectively. Semiconductors are used in solar cells to convert solar radiation into electrical energy. Photons with energy higher than their band gap will be absorbed by these materials when they are exposed to light. To reach the cell junction and produce electricity, a photon must first remove an electron from its atom. The transformation of light energy (photons) into electrical energy (voltage) is known as the photovoltaic effect.

The mathematical analysis of the selected PV model parameters based on the information in Table 3.5 is given by the following equations. The short circuit or series resistance is chosen after taking into account the open circuit voltage, the modules' maximum peak voltage, and the maximum peak current.

$$R_s = \frac{V_{oc} - V_{mp}}{I_{mp}} = \frac{49.7 - 41.2}{13.35} = 0.637 \ \ ohm \tag{3.27}$$

Also, the shunt resistance is determined as follows in Equation (3.27):

$$R_{sh} = \frac{I_{sc}R_s - V_{oc}}{I_{mp} - I_{sc}} = \frac{(13.7 * 0.637) - 49.7}{13.35 - 13.7} = 117.07 \ ohm \tag{3.28}$$

MATLAB/Simulink is used to model a PV array based on the mathematical equation for the solar system. The relevant parameters for PV array modeling, including Isc, G, Ns, Np, Kt, Tref, and Voc, were taken from the standalone system's PV module description and are displayed in Table 3.4. The PV array is represented by a number of irradiances at a constant temperature. The actual output voltage and current are computed using the series and parallel PV modules identified by the analysis in the preceding section.

$$V_{pv} = V_{mpp\ module} * N_s = 41.2 * 19 = 782.8 \ \ V \tag{3.29}$$

$$I_{pv} = I_{mpp\ module} * N_p = 13.35 * 27 = 360.45 \ \ A \tag{3.30}$$

3.1.4 Modeling of DC-DC Boost Converter

DC-to-DC converters come in three main varieties: buck, boost, and buck-boost. The boost converter will be the focus of our analysis. The complete circuit diagram and the calculated values for its four main parts the resistor, diode, capacitance, and inductance are shown in Figure 3.9. Assuming an input voltage of 780V and a switching frequency of 10 kHz, As a result, the output voltage Vo in the DC-DC boost converter design is 800V, with a common stable DC bus voltage of 480V AC and a motor load of 238 kW. The diode is a crucial part that protects the PV array by stopping negative current from passing through it. A capacitor is also used to reduce high-frequency harmonics.

The condition of the switch determines how the boost converter operates:

- Switch Closed (ON State): The input voltage (Vin) and the voltage across the inductor (VL) are equal when the switch is closed. The inductor's current increases linearly over this period. Since the diode is reverse-biased, current cannot pass through it.
- Switch Opened (OFF State): Regardless of any voltage drop across the diode, the voltage across the inductor (VL) becomes Vin−Vo when the switch opens. The diode becomes forward-biased in this condition, permitting current to flow. The inductor current now drops as opposed to rising in the ON state.

Step 1: Calculation of duty cycle:

$$V_o = \frac{V_s}{1-D} \tag{3.31}$$

where Vin is the converter's PV input voltage, Vo is its output voltage, and D is its duty cycle. The greatest duty ratio required to obtain the 600-volt output voltage can be demonstrated by rearranging equation (3.31).

$$D = 1 - \frac{V_{in}}{V_o} = 1 - \frac{780V}{800\,V} = 0.025\ or\ 2.5\ \% \quad (3.32)$$

Since determining the DC load requires knowing the output power, the following formula is used to calculate the DC load resistance:

$$R = \frac{{V_o}^2}{P} = \frac{780^2}{238000} = 2.55\ ohm \quad (3.33)$$

The following formula can be used to calculate the average input current and the inductor voltage:

The filter inductor value and peak current are determined using the given maximum inductor current ripple.

$$I_{in} = {P_{out}}/{V_{in}} = {282150W}/{780V} = 361.7A \quad (3.34)$$

$$L = \frac{D*V_{in}}{2*F_s*\Delta I_l} = \frac{780V*0.025}{36.17A*2*10000} = 2.7\ micro\ henry \quad (3.35)$$

Step 2: The following formula is also used to calculate the minimum capacitor value.

The capacitor passes a constant output voltage while filtering the inductor current ripple. The regulator must additionally confirm that load steps at the output are supported before it may respond.

where r is the ripple factor of the boost converter's output voltage. Since it is thought to be no more than 1%, the ripple voltage will be 8 volts.

$$I_{out} = {P_{out}}/{V_{out}} = {282150}/{800} = 352.7A \quad (3.36)$$

$$C = \frac{D * I_{out}}{2 * f_s * \Delta V_{out}} = \frac{352.7A * 0.025}{2 * 10000HZ * 8V} = 5\ Micro\ farad \quad (3.37)$$

where L is the load's inductance (H), R is its resistance (Ω), fs is its switching frequency (Hz), and D is its duty cycle (%).

Table 3. 6: The boost converter's chosen parameter

Parameter	Symbol	Values
Input voltage	V_{mpp}	780 V
Duty ratio	D	0.025
Inductor	L	2.7 $micro\ Henry$
Load resistance	R	2.55 ohm
Output capacitor	C_o	5 μF
Switching frequency	f_s	10 kHz

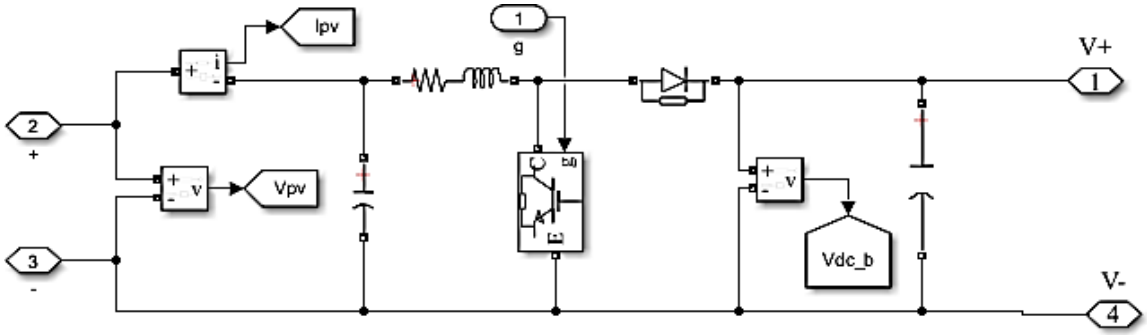

Figure 3. 7: Modeling of the boost converter

3.1.5 Inverter Sizing

The inverter must be sized to manage the maximum expected power of the AC load. **Selection:** for redundancy, employing numerous inverters is preferable. Assume that the rated AC power load is 238 kw and that there are two inverters, each rated at 125 kw AC, totaling 250 kw. For inverters, the array split is 27 strings between two inverters.

Inverter 1 has 13 strings and 13 * 19 * 550 W, or 135.85 KW of power. Inverter 2 has 14 strings and 14*19*550W of power, or 146.3 KW.

Current per inverter:

Inverter 1: Imp *13=13.35A*13=173.55 A

Inverter 2: Imp *14=13.35A*14=186.9 A

3.1.5.1 Analysis of DC Link Capacitor

This method of determining the minimum capacity of the DC link capacitor requires the evaluation of the maximum input power step and the determination of the maximum permitted voltage deviation. A common constraint is a 10% DC link voltage variation at any step-on and step-off load response. The power of the solar panel at its maximum power point (MPP) is the same as the anticipated maximum input power step. The DC/DC converter's control delay is represented by the time constant Tr, and a value of, say, five to ten modulation periods is a reasonable choice. The energy ΔW is first calculated as follows:

$$\Delta W = \int_0^{Tr} \Delta P_{max} d_t = \Delta P_{max} T_r \qquad (3.38)$$

The following is an expression for the energy stored by the capacitor:

$$W = \frac{1}{2} C_d {V_d}^2 \qquad (3.39)$$

Additionally, depending on the DC link voltage V_d, the DC link voltage deviation ΔV_d, and the capacity C_d, the fluctuation of the capacitor's stored energy can be approximated as follows:

$$\Delta W = \frac{1}{2} \boldsymbol{C}_{\boldsymbol{d}(\boldsymbol{V_d}+\Delta \boldsymbol{V_d})^2 - \frac{1}{2}\boldsymbol{C_d}{\boldsymbol{V_d}}^2} \qquad (3.40)$$

The minimal capacity $C_{d,min}$ is expressed as the combination of Equations (3.38) and (3.39):

$$V_{d.min} \geq \frac{T_r P_{max}}{\left(V_d \Delta V_d + \frac{1}{2} {\Delta V_d}^2\right)} \qquad (3.41)$$

The following approximation of the energy ΔW transported by the capacitor bank offers an additional means of comprehending the minimum DC link capacity:

$$\Delta W = \frac{T_r \Delta P_{max}}{2} \quad (3.42)$$

The voltage deviation is given by:

$$\Delta V_{d=} \frac{\Delta W}{C_d V_d} \quad (3.43)$$

This results in the following equation for the minimum capacity, $V_{d.min}$:

$$V_{d.min} \geq \frac{T_r P_{max}}{2 V_d \Delta V_d} \quad (3.44)$$

It is possible to compare equations (3.43) and (3.44) and see that the increase in yields values that are roughly twice as high as the minimal capacity. by making the widely accepted assumption that the DC link voltage deviation Vd is 10%.

3.2 Maximum Power Point Tracking (MPPT) Controllers for Photovoltaic Systems

The output of solar photovoltaic (PV) panels is very susceptible to weather fluctuations, which means that their maximum efficiency can only be attained at a particular electrical operating point. Methods for Maximum Power Point Tracking (MPPT) are therefore essential. These algorithms are crucial for continuously altering the PV system's operation to extract the most power, regardless of changes in solar irradiation and other environmental factors. Maximum electricity Point Tracking (MPPT) controllers are essential components of photovoltaic (PV) systems because they maximize the amount of electricity generated by solar panels under a range of environmental conditions. The Maximum Power position (MPP) is a unique operating position at which solar panels produce their maximum amount of power. This MPP is not constant; it varies according to variations in temperature, solar irradiation, and even load factors.

Why MPPT is Crucial

A solar panel's voltage and current have a non-linear connection. Significant power losses could result from a solar panel operating at a point on its current-voltage (I-V) curve that is far from its MPP in the absence of an MPPT controller. To guarantee that the solar panels provide the load or battery bank with the most power possible, MPPT controllers continuously modify the electrical operating point of the panels. Depending on the circumstances, this adjustment can greatly boost a PV system's efficiency, frequently by 10–30% or even more.

MPPT controllers are essentially DC-to-DC converters (like boost or buck converters) that use intelligent algorithms to find and maintain the MPP. They closely monitor the output voltage and current from the solar panels. Based on these readings, the controller determines the optimal voltage and current for the panels to operate at in order to generate the maximum amount of power. In order to maximize power transfer, it then modifies its internal circuitry to "match" the panel's output to the demands of the load or battery, transforming any excess voltage into increased current or vice versa.

Key functions of an MPPT controller include:

The main role is to track the MPP. The MPP is found by algorithms that continually scan the panel's I-V curve.

Voltage and Current Adjustment: In order to maximize the current delivered and effectively charge batteries or power loads at the necessary voltage, they adjust the voltage from the solar panels.

Battery Management: In order to prolong battery life, many MPPT controllers additionally include battery charging algorithms that offer temperature correction and guard against overcharging and over discharging System. safety often includes features like overcurrent protection, short-circuit protection, and reverse polarity protection.

3.2.1 ANFIS based MPPT controller

ANFIS-based MPPT controllers efficiently track the maximum power point (MPP) of solar PV arrays by utilizing the benefits of fuzzy logic and neural networks. Input signals that the PV array

uses to operate include its voltage and current, as well as perhaps environmental data like temperature and solar irradiation. The ANFIS model's fuzzy logic, which defines how various inputs connect to the intended optimal operating point via linguistic rules, is its fundamental component. A key component is the learning technique used by the controller to train the neural network component.

To reduce differences between the controller's output and the actual power output, the system's settings are changed during this training phase. After completing its training, the ANFIS controller generates the MPP. This allows it to modify the load impedance or other control parameters to guarantee that the PV array produces the most power possible.

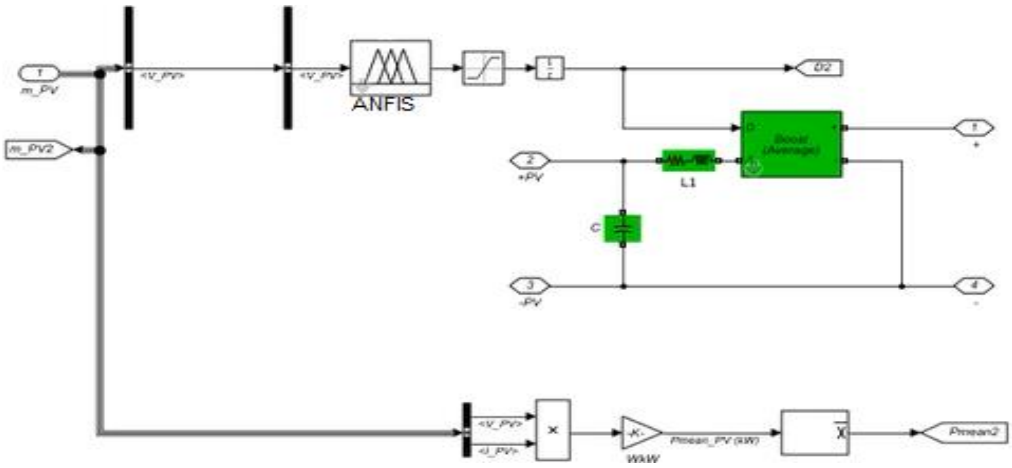

Figure 3.8: Simulink model of ANFIS based MPPT controller

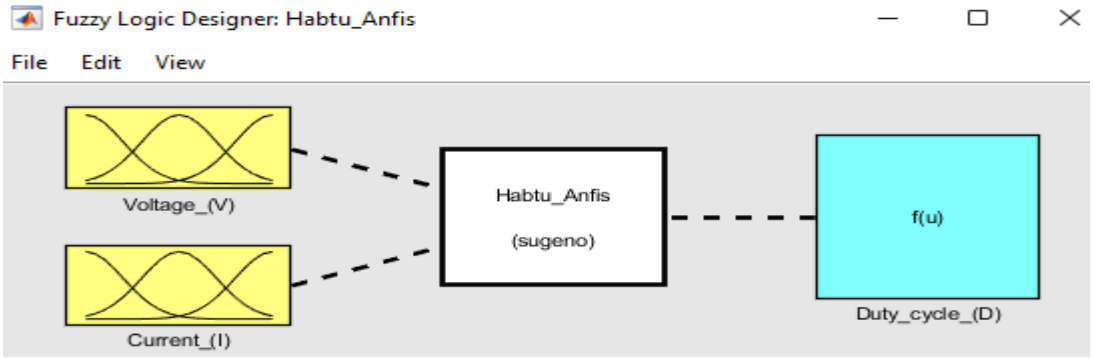

Figure 3. 9: Input and output variables with fuzzy logic designer

The construction of an ANFIS controller in a fuzzy logic environment is shown in Figure 3.9. It graphically depicts the system's inputs, voltage (V) and current (I), which are processed by the Sugeno type ANFIS to produce duty cycle (D), the only output.

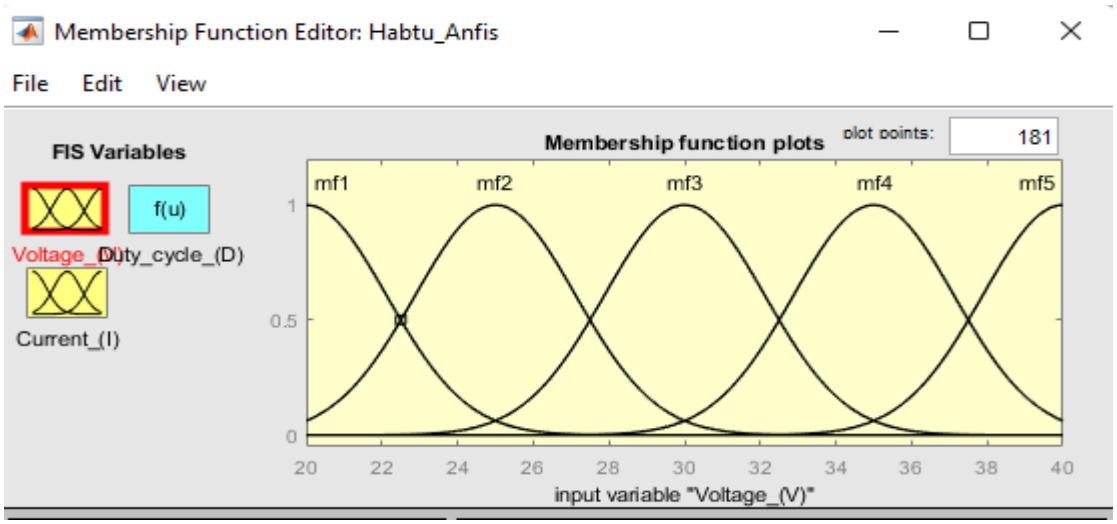

Figure 3.10: Membership functions of input variable Voltage

Figure 3.10 displays the membership functions for the "Voltage V" input variable within the system. It shows five overlapping Gaussian-like membership functions (mf1 to mf5) defining the fuzzy sets for voltage over a range of approximately 20 to 40 units.

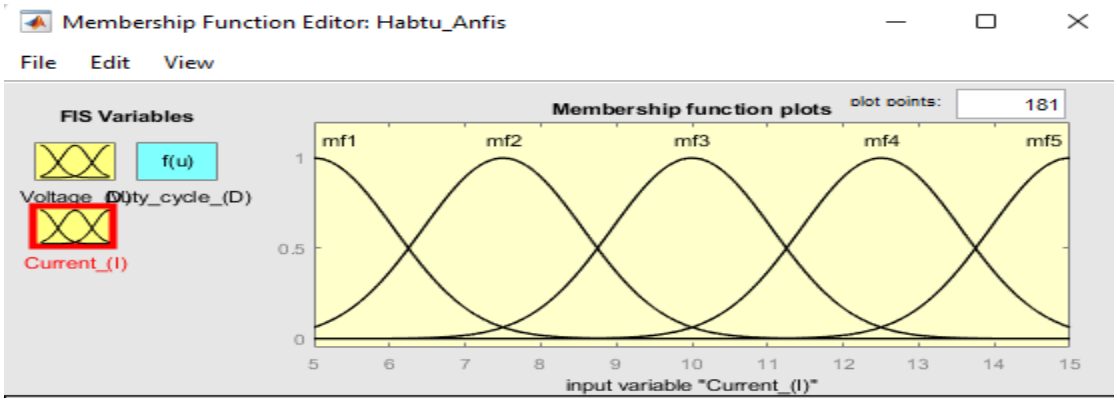

Figure 3.11: Membership functions of input variable Current

Similar to the previous one, Figure 3.11 shows the membership functions for the "Current I" input variable within the system. It displays five overlapping Gaussian-like membership functions (mf1 to mf5) defining the fuzzy sets for current over a range of approximately 5 to 15 units.

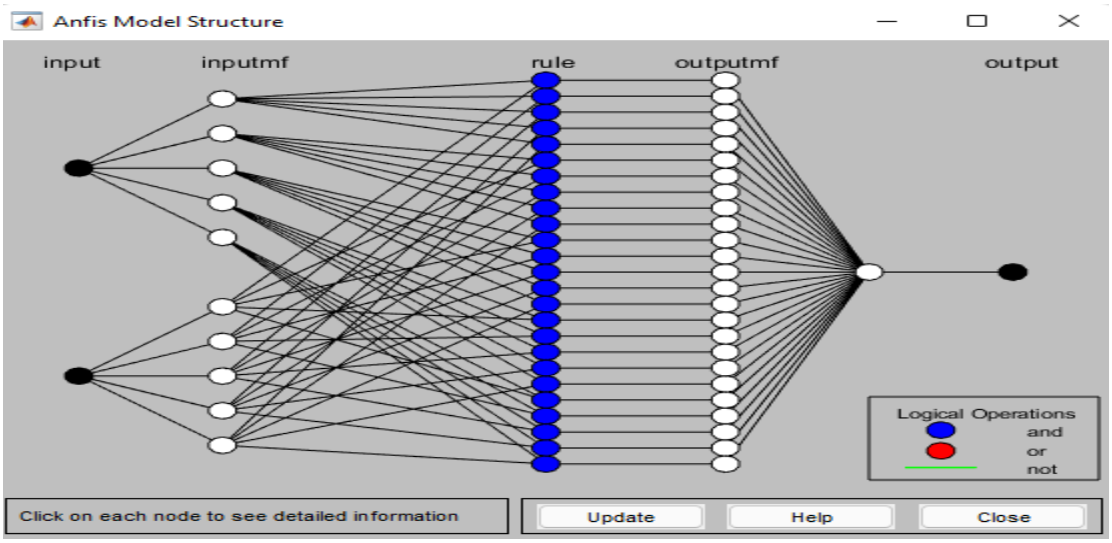

Figure 3.12: ANFIS model structure

Figure 3.12 shows a typical adaptive neuro-fuzzy inference system with a five-layer architecture. As a visual representation of the interrelated levels of the ANFIS model, it shows two input nodes, their corresponding input membership functions, a layer of fuzzy rules (represented by blue nodes for 'and' operations), output membership functions, and a single output node.

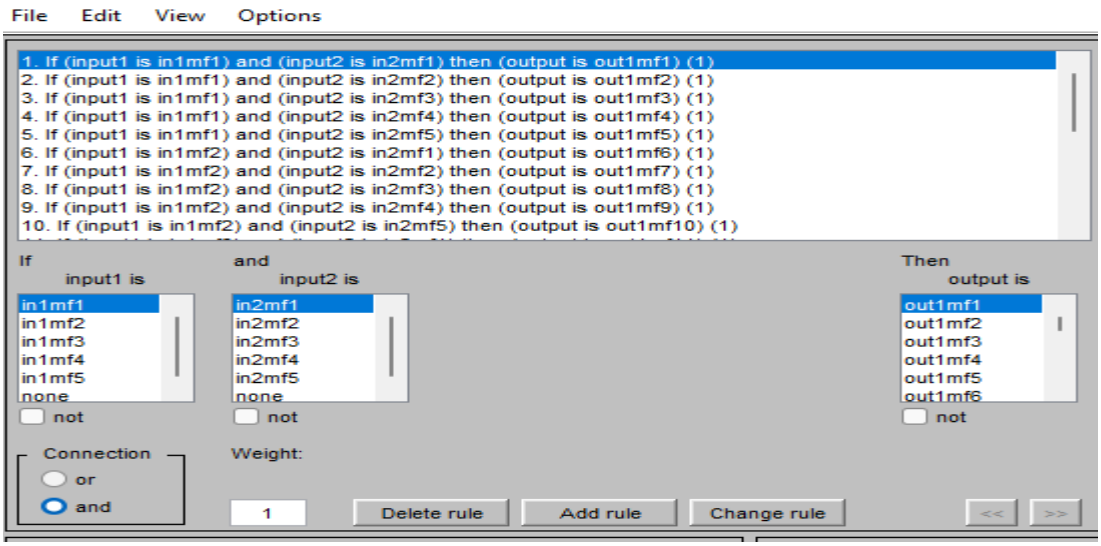

Figure 3.13: Fuzzy rules for the system

This Figure 3.13 shows a "Rule Editor" for a fuzzy logic system, specifically displaying a partial list of "If-Then" rules. Each rule connects fuzzy sets from two inputs ("input1" and "input2," likely corresponding to voltage and current) using an "and" connection, to a specific fuzzy output

("output" or "Duty cycle"). The screenshot illustrates the first ten rules, indicating a systematic mapping between input conditions and desired outputs.

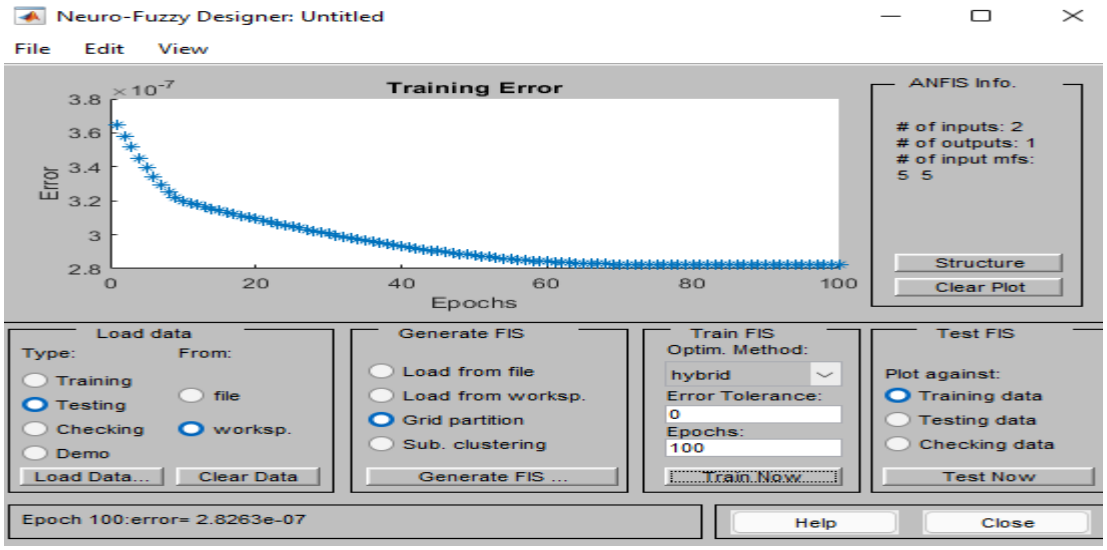

Figure 3.14: Training error with epoch 100

Figure 3.14 shows the training performance of an ANFIS model. The main "Training Error" plot illustrates a decreasing error over 100 epochs, indicating that the ANFIS model successfully learned from the data. The "ANFIS Info" panel confirms the model has two inputs, one output, and five membership functions for each input.

3.2.2 The PV MPPT controllers perturb and observe (P&O) algorithm

The Perturb and Observe (P&O) method for PV-MPPT has become widely used because to its simplicity and low cost. However, it has limitations such drift vulnerability, large power fluctuations near the Maximum Power Point (MPP), and poor tracking, especially when there is fast variation in solar irradiation.

The Incremental Conductance (IC) MPPT approach was created to overcome these shortcomings and provide better performance in rapidly changing environmental conditions. Notwithstanding its benefits, measurement mistakes and the intrinsic usage of derivative operations might make the IC technique prone to errors. Both P&O and IC approaches have seen a number of revisions, however they frequently only offer partial answers.

Consequently, artificial intelligence (AI) techniques such as fuzzy logic control (FLC) and artificial neural networks (ANN) have emerged as more dependable alternatives. Without the need for precise system parameters or complex mathematical models, these AI-based techniques provide increased accuracy and flexibility, particularly for the non-linear behavior of PV systems. A flowchart, like the one in Figure 3.15, is commonly used to illustrate the P&O algorithm's operating flow.

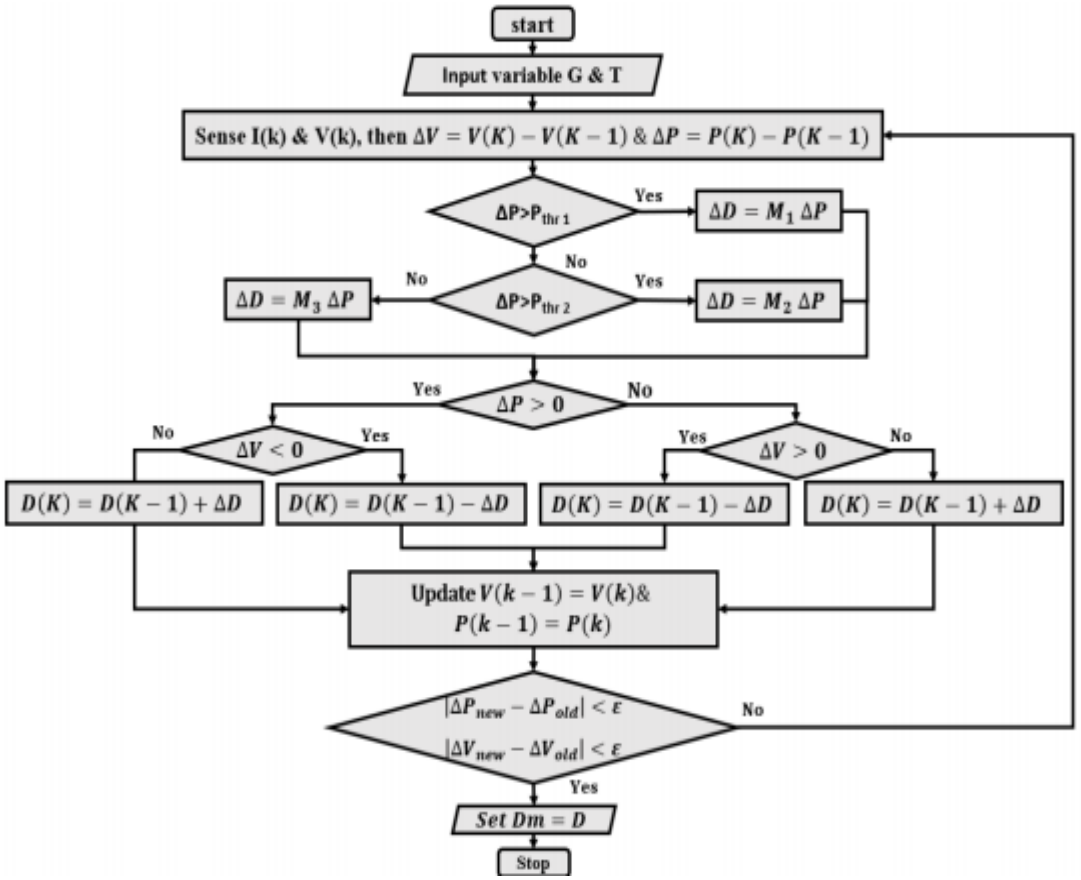

Figure 3.15: P&O algorithm flowchart for PV MPPT controller

This flowchart, Figure 3.13, details the operation of an enhanced Perturb and Observe (P&O) algorithm for PV MPPT. It demonstrates how the system continuously measures PV voltage and current, computes power variations, and adaptively modifies the duty cycle in response to these variations and preset thresholds in order to monitor the Maximum Power Point. In order to stabilize the duty cycle after the MPP is reached, the method additionally includes a convergence check.

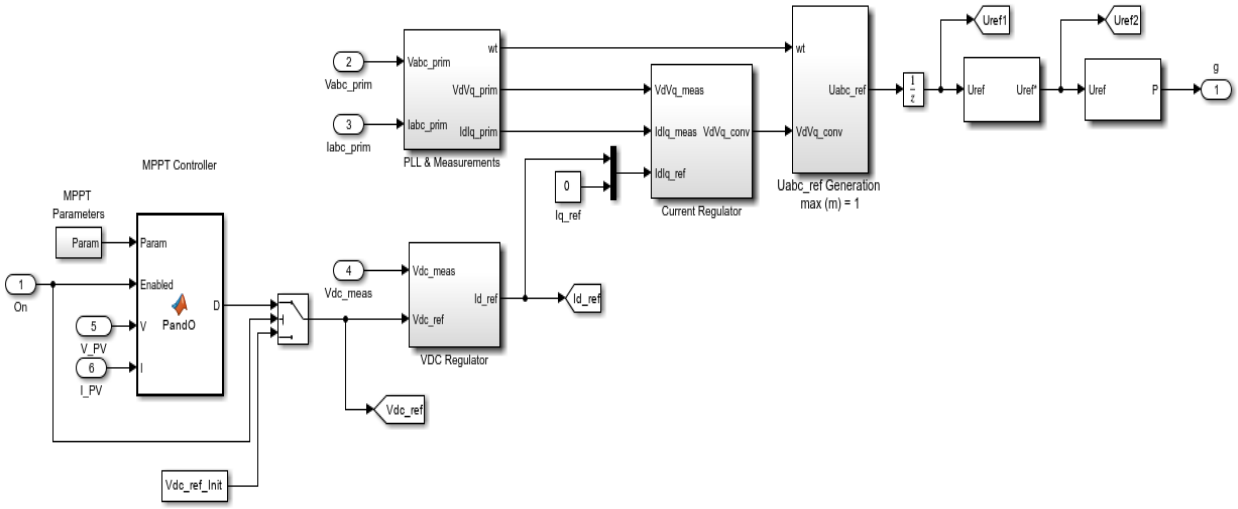

Figure 3.16: P&O algorithm Simulink representation with MATLAB function block diagram

Figure 3.16 displays the Perturb and Observe (P&O) MPPT method as a Simulink model that incorporates a MATLAB Function block. The P&O algorithm, which generates a duty cycle that controls a DC-DC converter (shown by the switch), uses the PV voltage and current as inputs. The model is utilized in a motor drive system, as seen by the addition of components for voltage regulation, current regulation, and AC reference generation.

3.2.3 Permanent magnet synchronous motors for water pumping system

Because Ethiopia's agriculture depends on irrigation, a solar PV-powered pumping system is a particularly relevant and sustainable alternative. High-performance and high-efficiency motor drives are commonly powered by permanent magnet synchronous motors (PMSM). High-performance motor control features include swift acceleration and deceleration, total torque control at zero speed, and smooth spinning over the motor's whole speed range.

The magnetic power of the motor determines how DC-excited and non-excited synchronous motors operate. Permanent magnet motors, hysteresis motors, and reluctance motors are examples of non-excited synchronous motors. Permanent Magnet Synchronous Machines (PMSM) have solidified their supremacy over other machine types in the motor drive industry during the last few

decades. Because of their unique qualities, PMSM drives are utilized in almost every industry, from home appliances to vehicle propulsion. These features include high efficiency, high torque, and high power density.

The permanent magnet, which may be viewed as an energy source, is responsible for PMSM's high power density. However, it also irritates since the magnetic field it produces is quite fixed. For high-speed applications, flux-weakening, often referred to as field-weakening, is almost always required for PMSM drives. In the flux-weakening zone, issues including low torque control accuracy, unstable current management, and a limited constant power speed ratio continue to exist, making the use of advanced control strategies that can improve PMSM performance throughout a wide speed and torque range necessary.

The torque and speed control techniques proposed in this dissertation improved existing PMSM control strategies in the flux-weakening domain. To address the current oscillation issue with the voltage-regulated flux-weakening controller, the current trajectory was changed and the operating region was extended to the Maximum Torque per Volt (MTPV) region. To provide accurate torque control in the flux-weakening zone, an open-loop torque controller was proposed. Together with this controller, a special PMSM characterization test technique was developed to recover PMSM machine data. The results of this characterization test also led to the development of a new high fidelity PMSM modeling method that can capture the nonlinearity of PMSM machines.

All of the control strategies proposed in this study are applicable to interior-mounted (SPM) or surface-mounted (IPM) permanent magnet synchronous machines.

One method for managing the PMSM is field-oriented control (FOC). Since the position and amplitude of the field flux are known, the controller in vector control can control the armature flux amplitude and angle with respect to the field flux. The rotor magnetic field created by permanent magnets produces a sinusoidal rate of change of flux, which is dependent on the rotor angle. When the rotor angle defining parameter is set to the angle between the a-phase magnetic axis and the d-axis, the a-phase and permanent magnet fluxes align when the rotor mechanical angle, θr, is zero,

in accordance with the axes convention. When the angle between the a-phase magnetic axis and the q-axis is chosen as the rotor angle defining parameter, the rotor mechanical angle is the angle between a phase magnetic axis and the rotor q-axis.

3.2.3.1 abc to αβo to dqo and to abc voltages and currents transformation

The reduction of system complexity is the primary advantage of dq transformation. By employing Idq to independently control torque and flux, decoupling can be accomplished.

The transformation essentially aids in controlling a portion of motor drives, but rotor position is necessary for optimal PID controller operation.

- The ABC to Alpha-Beta-Zero block performs a Clarke transform on a three-phase ABC signal. An inverse Clarke transform is applied to the αβ0 components in the Alpha-Beta-Zero to ABC block.
- This part carries out Clarke's transformation, which is the ABC to αβγ transformation. When the three-phase system is balanced, this transformation projects the three-phase quantities onto two stationary axes. This transformation occurs in three modes:
- Variant power: Clarke's original: Edith Clarke's original metamorphosis. This result equals the zero-sequence derived from the transformation of the symmetrical component because the γ axis is flattened. Because the transformation matrix is not unitary, this transformation is a power variation.
- Variant power-uniform: A modification of Clarke's first transformation that maintains uniformity across all axes. This output differs from the zero sequence of the transformation of the symmetrical component because the γ axis is not squashed. The power is variable since the transformation matrix is not unitary.
- With a unitary transformation matrix, invariant power is an adaptation of Clarke's original transformation that maintains uniformity across all axes. Following this change, the power calculation is identical to the calculation that was performed initially. This output differs from the zero sequence of the transformation of the symmetrical component because the γ axis is not squashed.

The following points briefly addresses our concerns to perform the abc-to-dqo transformation:

- The three-phase instantaneous voltages and currents are converted into the synchronously rotating reference dqo frame to facilitate computations. Second, it allows the system operator to control the active (d-axis) and reactive (q-axis) components of the currents separately. Similarly, the machine's aspect's torque and flux can be controlled independently. This can significantly lessen the coupling effect.
- Furthermore, the mutual inductance is constant in the dqo-frame. Because the inductance-dependent variables are constant, the system operator can thus attain the intended output.
- Additionally, when the quantities are DC (i.e., constant), the different feedback controllers, such as proportional-integral (PI) and proportional-integral-derivative (PID), practically provide an efficient and dependable control solution. Conversely, the integrator (i.e., 1/S) term of these feedback controllers usually fails to introduce the infinite gain if the input quantities given to them are sinusoidal or periodic. Consequently, there will be no forcing of the steady-state error to zero.

Park transformation

- This is the most important transformation in FOC
- The two-phase fixed orthogonal system (α, β) is transformed into a d,q rotating reference frame by this projection.
- The transformation matrix is given below

Here eq (3.45) is αβo currents transformation to dqo currents using Park transformation

$$I_d = I_\alpha \cos(\theta) + I_\beta \sin(\theta)$$
$$I_q = I_\beta \cos(\theta) - I_\alpha \sin(\theta)$$

$$I_\alpha = \frac{2}{3}(I_a) - \frac{1}{3}(I_b - I_c)$$

$$I_\beta = \frac{2}{\sqrt{3}}(I_b - I_c)$$

For a simplified case when $I_a + I_b + I_c = 0$:

$$I_\alpha = I_a$$

$$I_\beta = \frac{1}{\sqrt{3}}(2I_b + I_a)$$

$$\begin{bmatrix} d \\ q \\ 0 \end{bmatrix} = \frac{2}{3}\begin{bmatrix} \sin(\theta) & \sin(\theta - \frac{2\pi}{3}) & \sin(\theta + \frac{2\pi}{3}) \\ \cos(\theta) & \cos(\theta - \frac{2\pi}{3}) & \cos(\theta + \frac{2\pi}{3}) \\ \frac{1}{2} & \frac{1}{2} & \frac{1}{2} \end{bmatrix}\begin{bmatrix} a \\ b \\ c \end{bmatrix} \tag{3.45}$$

$$i_{\alpha\beta\gamma}(t) = \sqrt{\frac{2}{3}}\begin{bmatrix} 1 & -\frac{1}{2} & -\frac{1}{2} \\ 0 & \frac{\sqrt{3}}{2} & -\frac{\sqrt{3}}{2} \\ \frac{1}{\sqrt{2}} & \frac{1}{\sqrt{2}} & \frac{1}{\sqrt{2}} \end{bmatrix}\begin{bmatrix} i_a(t) \\ i_b(t) \\ i_c(t) \end{bmatrix}$$

$$\begin{bmatrix} i_a(t) \\ i_b(t) \\ i_c(t) \end{bmatrix} = \begin{bmatrix} 1 & \\ -\frac{1}{2} & \frac{\sqrt{3}}{2} \\ -\frac{1}{2} & -\frac{\sqrt{3}}{2} \end{bmatrix}\begin{bmatrix} i_\alpha(t) \\ i_\beta(t) \end{bmatrix} \tag{3.46}$$

$$I_\alpha = I_d\cos(\theta) - I_q\sin(\theta)$$

$$I_\beta = I_d\sin(\theta) + I_q\cos(\theta)$$

Here also in eq (3.46) clearly shows abc currents transformation to αβo currents

	Standard (Amplitude-Invariant)	Power-Invariant
Clarke abc to $\alpha\beta 0$	$\frac{2}{3}\begin{bmatrix} 1 & -\frac{1}{2} & -\frac{1}{2} \\ 0 & \frac{\sqrt{3}}{2} & -\frac{\sqrt{3}}{2} \\ \frac{1}{2} & \frac{1}{2} & \frac{1}{2} \end{bmatrix}$	$\sqrt{\frac{2}{3}}\begin{bmatrix} 1 & -\frac{1}{2} & -\frac{1}{2} \\ 0 & \frac{\sqrt{3}}{2} & -\frac{\sqrt{3}}{2} \\ \frac{1}{\sqrt{2}} & \frac{1}{\sqrt{2}} & \frac{1}{\sqrt{2}} \end{bmatrix}$
Park abc to $dq0$	$\frac{2}{3}\begin{bmatrix} \cos(\theta) & \cos(\theta - \frac{2\pi}{3}) & \cos(\theta + \frac{2\pi}{3}) \\ -\sin(\theta) & -\sin(\theta - \frac{2\pi}{3}) & -\sin(\theta + \frac{2\pi}{3}) \\ \frac{1}{2} & \frac{1}{2} & \frac{1}{2} \end{bmatrix}$	$\sqrt{\frac{2}{3}}\begin{bmatrix} \cos(\theta) & \cos(\theta - \frac{2\pi}{3}) & \cos(\theta + \frac{2\pi}{3}) \\ -\sin(\theta) & -\sin(\theta - \frac{2\pi}{3}) & -\sin(\theta + \frac{2\pi}{3}) \\ \frac{1}{\sqrt{2}} & \frac{1}{\sqrt{2}} & \frac{1}{\sqrt{2}} \end{bmatrix}$
Inverse Clarke $\alpha\beta 0$ to abc	$\begin{bmatrix} 1 & 0 & 1 \\ -\frac{1}{2} & \frac{\sqrt{3}}{2} & 1 \\ -\frac{1}{2} & -\frac{\sqrt{3}}{2} & 1 \end{bmatrix}$	$\sqrt{\frac{2}{3}}\begin{bmatrix} 1 & 0 & \frac{1}{\sqrt{2}} \\ -\frac{1}{2} & \frac{\sqrt{3}}{2} & \frac{1}{\sqrt{2}} \\ -\frac{1}{2} & -\frac{\sqrt{3}}{2} & \frac{1}{\sqrt{2}} \end{bmatrix}$
Inverse Park $dq0$ to abc	$\begin{bmatrix} \cos(\theta) & -\sin(\theta) & 1 \\ \cos(\theta - \frac{2\pi}{3}) & -\sin(\theta - \frac{2\pi}{3}) & 1 \\ \cos(\theta + \frac{2\pi}{3}) & -\sin(\theta + \frac{2\pi}{3}) & 1 \end{bmatrix}$	$\sqrt{\frac{2}{3}}\begin{bmatrix} \cos(\theta) & -\sin(\theta) & \frac{1}{\sqrt{2}} \\ \cos(\theta - \frac{2\pi}{3}) & -\sin(\theta - \frac{2\pi}{3}) & \frac{1}{\sqrt{2}} \\ \cos(\theta + \frac{2\pi}{3}) & -\sin(\theta + \frac{2\pi}{3}) & \frac{1}{\sqrt{2}} \end{bmatrix}$

Figure 3.17: General transformation matrix from abc to αβo to dqo and vise-versa

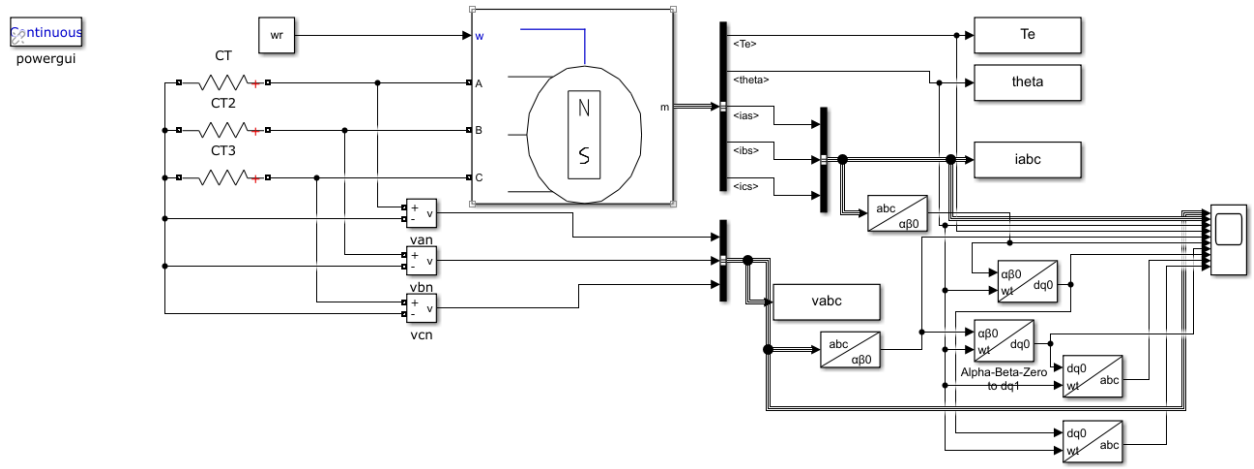

Figure 3.18: Simulink model of PMSM with abc voltages and currents to αβo to dqo voltages and currents transformation

A Simulink model of a permanent magnet synchronous motor (PMSM) is displayed in Figure 3.18. It is evident how to convert abc (three-phase) voltages and currents into dq0 (direct-quadrature-zero) and αβ0 (alpha-beta-zero) reference frames, which is crucial for control strategies like Field-Oriented Control.

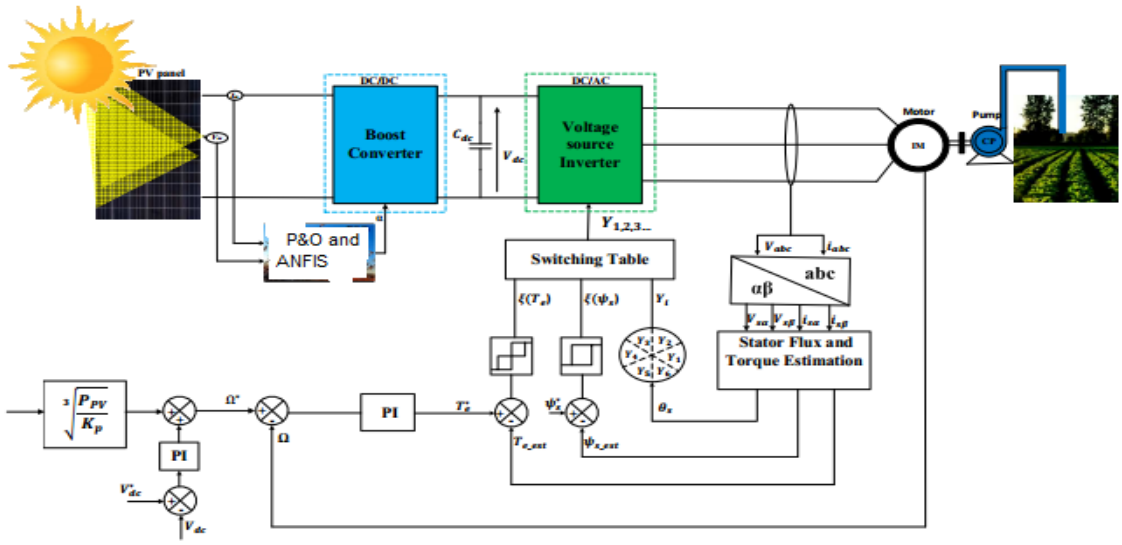

Figure 3.19: Architecture of the studied Photovoltaic Water Pumping System

Figure 3.19 depicts the design of a photovoltaic (PV) water pumping system. It displays a solar PV panel with a boost converter coupled to a voltage source inverter (VSI) that powers a water irrigation pump and an induction motor (IM). The system incorporates maximum power point tracking (MPPT) control methods using P&O and ANFIS, as well as a sensor-less direct torque control (DTC) scheme for the induction motor.

3.2.4 FOC based speed control of permanent magnet synchronous motor (PMSM) for PV based water pumping system

The FOC of an PMSM involves controlling the rotor and stator magnetic fields separately. The interaction between the rotor's magnetic field and the rotating magnetic field produced by the stator current causes the rotor to rotate. The rotor current is also controlled to produce a magnetic field that interacts with the stator's magnetic field to reduce slip and improve machine performance. The FOC technique can be applied to a mathematical model that describes the behavior of the induction machine. This model incorporates the dynamic equations for the rotor speed, electromagnetic torque, and stator and rotor currents. The model can be used to create controllers that regulate the rotor and stator currents and produce the necessary torque and speed.

Compared to other control systems, the FOC method has a number of advantages. FOC's ability to provide great performance and efficiency from the induction machine is one of its primary benefits. Slip is decreased and machine losses are minimized by controlling the rotor and stator magnetic fields independently.

The ability to precisely manage the machine's torque and speed is another benefit of FOC. This is crucial for applications requiring precise motor speed control, such industrial machinery and electric cars. When choosing a control technique, it's important to take into account the FOC method's restrictions. One of the key constraints of FOC is that it requires advanced control algorithms and technology. Advanced signal processing and control techniques are needed for FOC implementation, which can be difficult in particular situations. FOC's requirement for precise machine parameter knowledge, including rotor resistance and inductance values, is another drawback. Any mistakes in these settings could lead to imprecise control and worse machine

performance. Figure 3.20 displays the Simulink model of FOC PMSM as determined by the following diagram.

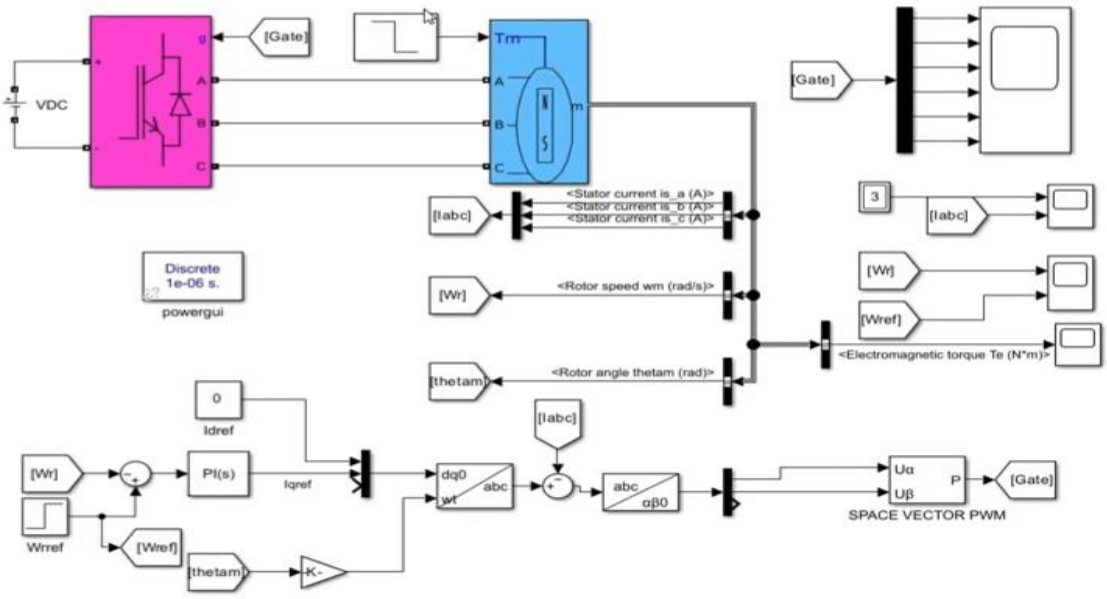

Figure 3.20: FOC PMSM Simulink model

Excellent dynamic performance is provided by the FOC IM Simulink model mentioned above, which is crucial for applications like robotics and automation that demand quick reaction times. The FOC approach can deliver the necessary torque and speed in a timely manner in response to variations in the load. The following Table 3.7 lists the parameters of the induction machine that was used for this simulation.

Table 3.7: PMSM simulation parameters

Parameter	Value	Parameter	Value
P	238 kW	Lm	0.4186
Rr	0.451	Line current	314A
Rs	1.2	Line voltage	480V

Lr	0.004125	Kp	16600
LS	0.004152	Ki	2700
f	50	J	0.05

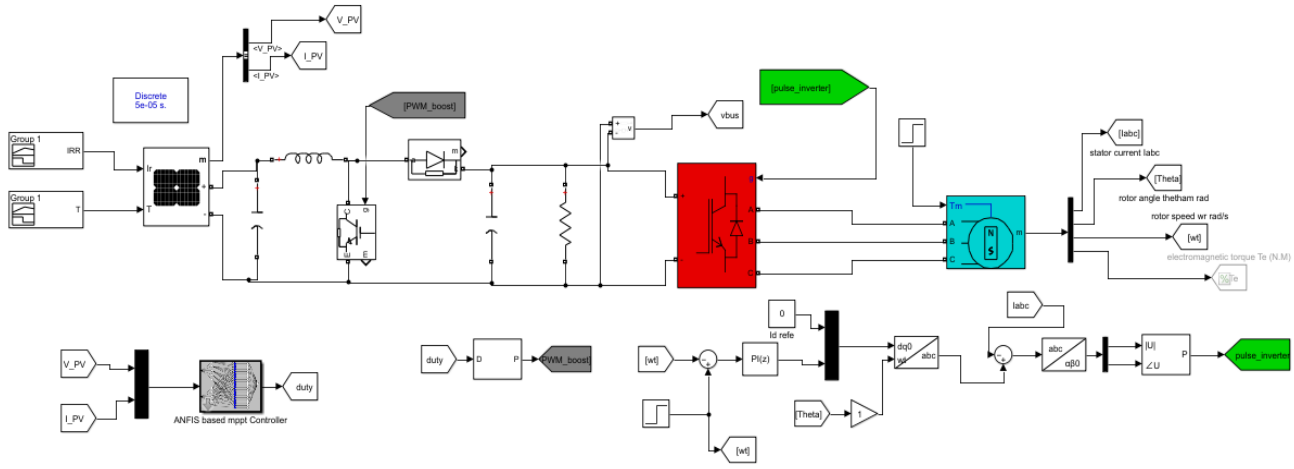

Figure 3.21: System's overall Simulink diagram

The detailed Simulink diagram of a solar PV-powered water pumping system is shown in Figure 3.21. In order to replicate the water pumping application, it shows the integration of a PV array, an electric motor (PMSM or IM), a power converter (probably a DC-AC inverter as it feeds a motor), and related control/measurement blocks.

CHAPTER 4

RESULTS AND DISCUSIONS OF SIMULATIONS

4.1 Simulation result of the PV analysis for site planning

These two graphs, which are shown in Figure 4.1 below, show the P-V (Power-Voltage) and I-V (Current-Voltage) characteristics of a photovoltaic module (or array) under different conditions, namely for a fixed irradiance of 1000 W/m² and a set open-circuit voltage (Voc) of 37.2V.

Using a high irradiance level of 1000 W/m² (Standard Test Conditions, or STC, which is commonly used for module ratings), a family of P-V (Power-Voltage) curves is shown in this graph. As the operating voltage changes, each colored line indicates the power output of the PV module (or a collection of modules).

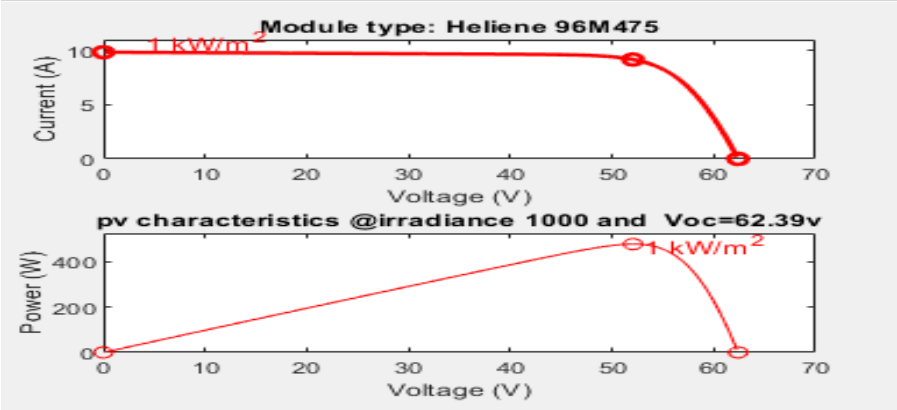

Figure 4. 1: Simulation result of PV system analysis of site planning for Amude in Arsi Ethiopia

4.2. The selected solar module PV and IV characteristics curve simulation result

One may evaluate the performance of the module, learn a lot about its behavior, and improve system operation and design by recreating the PV and Iv characteristics curve. Figure 4.2 below displays the outcomes of the simulation. Sensitivity assessments can be performed using simulation findings by altering variables like temperature and the impact of solar radiation. The

module's reaction to these changes and how they affect the IV characteristics curve might be the subject of discussions. This analysis supports system design and optimization by evaluating the module's performance in various environmental settings.

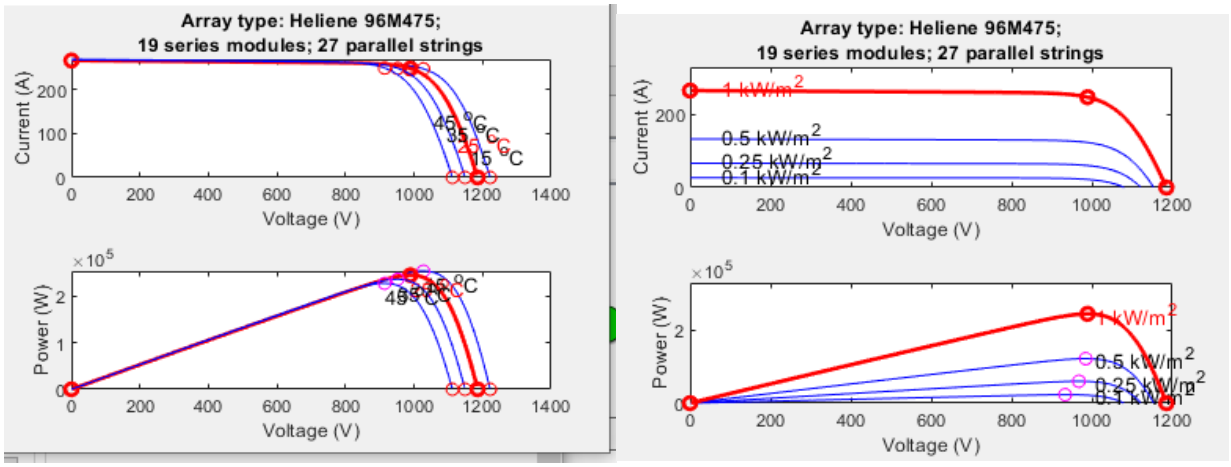

Figure 4. 2: PV and IV characteristic curves of the PV array

Figure 5.2 depicts the simulation results of the solar module's PV and IV characteristics curve provide crucial information about the module's performance, including MPP, Voc, Isc, fill factor (FF), efficiency, and sensitivity to environmental factors. These insights aid in system design, sizing, and optimizing the PV system's performance for a given application or scenario.

4.3 Simulation results of solar PV ANFIS based MPPT controller

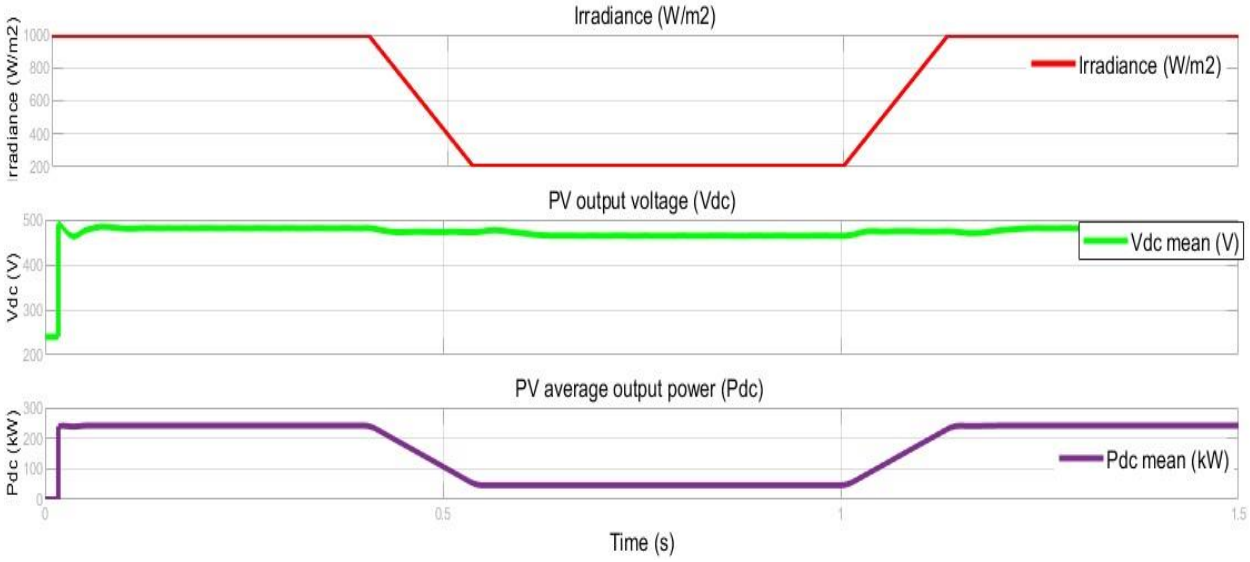

Figure 4. 3: Results of simulating the PV solar output irradiance, voltage, and average power using an MPPT controller based on ANFIS

Figure 4.3 of the simulation result shows the PV array's DC output voltage. When the irradiance is high, it begins at around 480V-490V, dips to about 470V-480V, when it drops to 200 W/m2, and rapidly returns to the starting voltage. when the irradiance reaches 1000 W/m². Despite large variations in irradiance, the voltage stays comparatively constant. One important sign of strong MPPT performance is this stability. An effective ANFIS-based MPPT controller would adjust the PV array's operating point (voltage and current) to maintain maximum power output because the voltage at which maximum power is achieved (Vmp) often doesn't fluctuate as much as current with irradiance.

The PV array's DC power output is displayed in this graphic. It begins at about 270 kW, dips precipitously to about 45 kW as the irradiance decreases, and then swiftly returns to 270 kW when the irradiance rises.

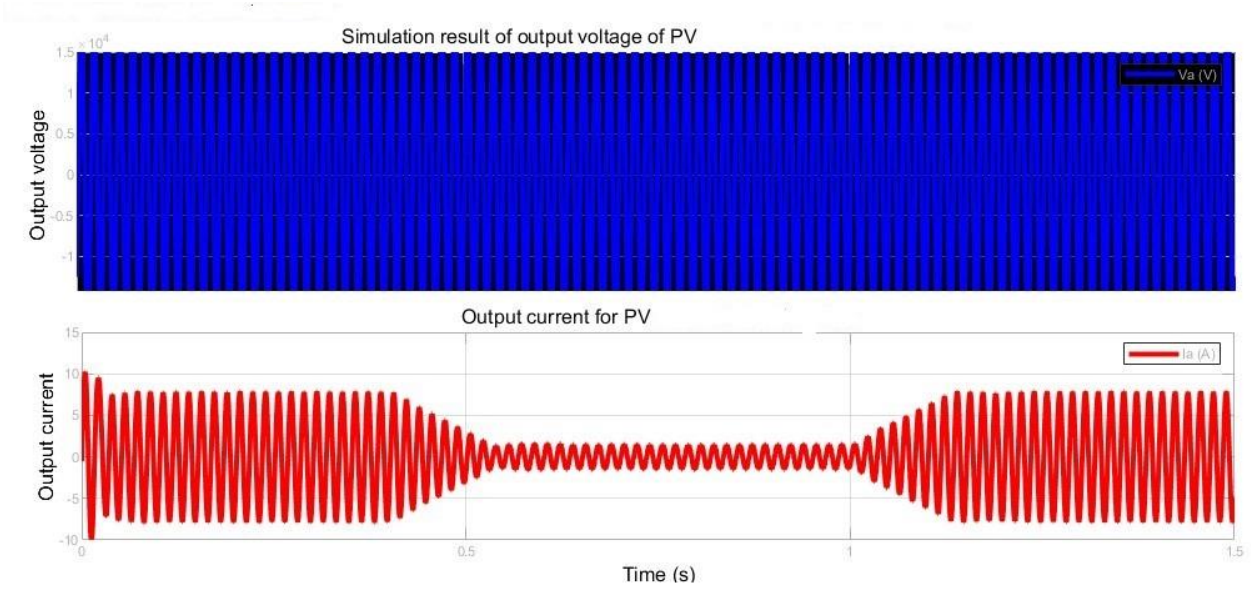

Figure 4. 4: Simulation results of output AC voltage and current from the PV with ANFIS

When analyzed for a water pumping application, the AC output voltage and current graphs in Figure 4.4 show that the system produces a steady sinusoidal AC voltage with corresponding current variations from a peak of roughly 10 A to 2-3 A, which exactly reflects the fluctuating solar power input. This suggests a highly extensive PV-powered AC water pumping system, which

calls for a sizable amount of water storage space in Amude to offset the natural fluctuations in pushed water volume brought on by shifting solar circumstances.

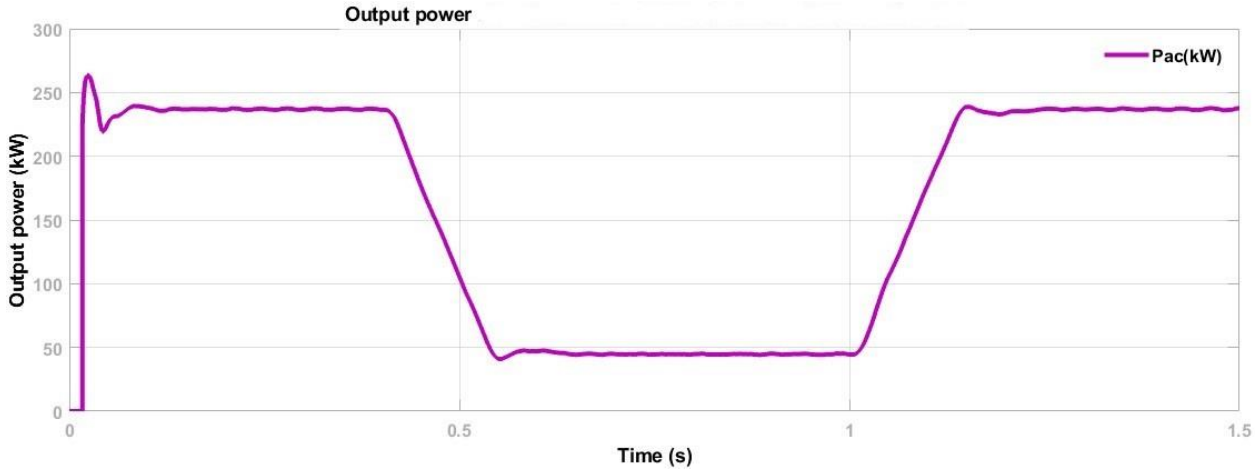

Figure 4. 5: The simulation result of AC output power for PV system with ANFIS

Assuming the PV system uses an inverter to drive an AC pump, the simulation graph shown in Figure 4.5 accurately depicts the AC power supplied to the water pump in Amude. The ANFIS MPPT simulation's irradiance and DC power variations closely resemble the observed power profile. The system's strong launch and steady-state performance under full sun (probably equivalent to 1000 W/m² irradiance) are demonstrated by the early surge to 260 kW and subsequent stabilization at 240 kW. A period of much lower solar irradiance is evident from the sharp decline in power from 240 kW to 45 kW between 0.4 and 1.1 seconds (as seen in the preceding irradiance graph dropping to 200 W/m²).

Once full solar input is restored, the system recovers quickly, as evidenced by the subsequent sharp climb back to 240 kW. The ANFIS MPPT controller controls this dynamic reaction, which guarantees that the water pump always gets the most power from the PV array. This has a direct effect on the water flow rate. The volume of water pumped will vary greatly with a power output ranging from 240 kW to 45 kW, underscoring the critical need for a large water storage reservoir in Amude to ensure a consistent and reliable water supply independent of immediate solar changes.

4.4 Simulation results of solar PV P&O algorithm based MPPT controller

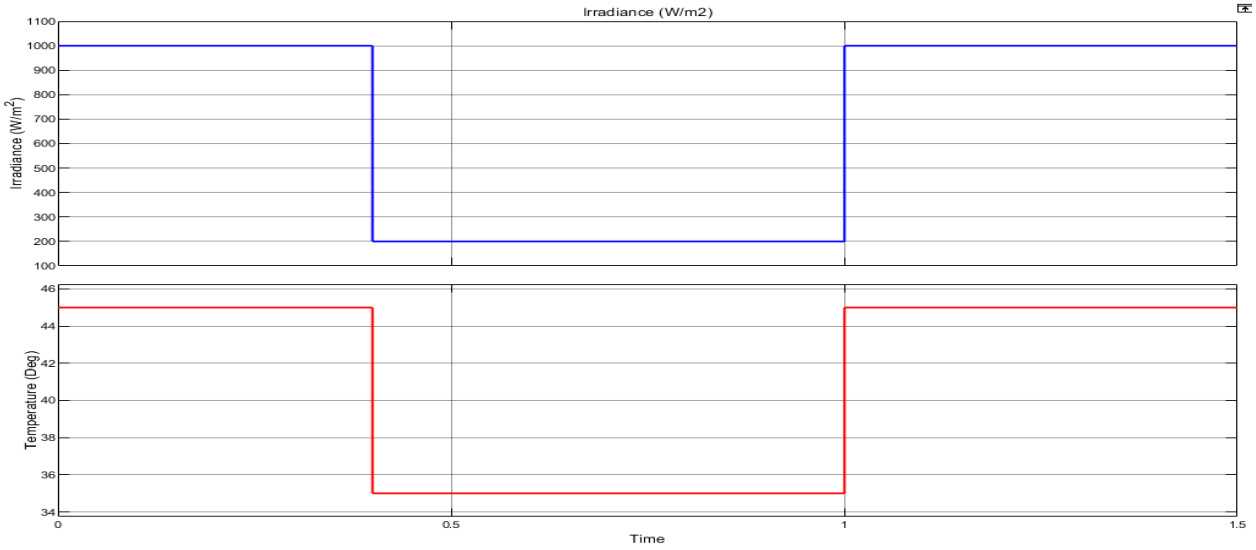

Figure 4. 6: Simulation results of output irradiance and temperature from the PV solar with P&O based MPPT controller

Figure 4.6 shows the output temperature and irradiance simulation results from a PV solar system with a P&O-based MPPT controller. Stepped changes in solar irradiance are shown in the top graph, which drops from 1000 W/m2 to 200 W/m2 and then rises again. Simultaneously, the bottom line displays equivalent stepped changes in temperature, which probably simulates natural environmental swings.

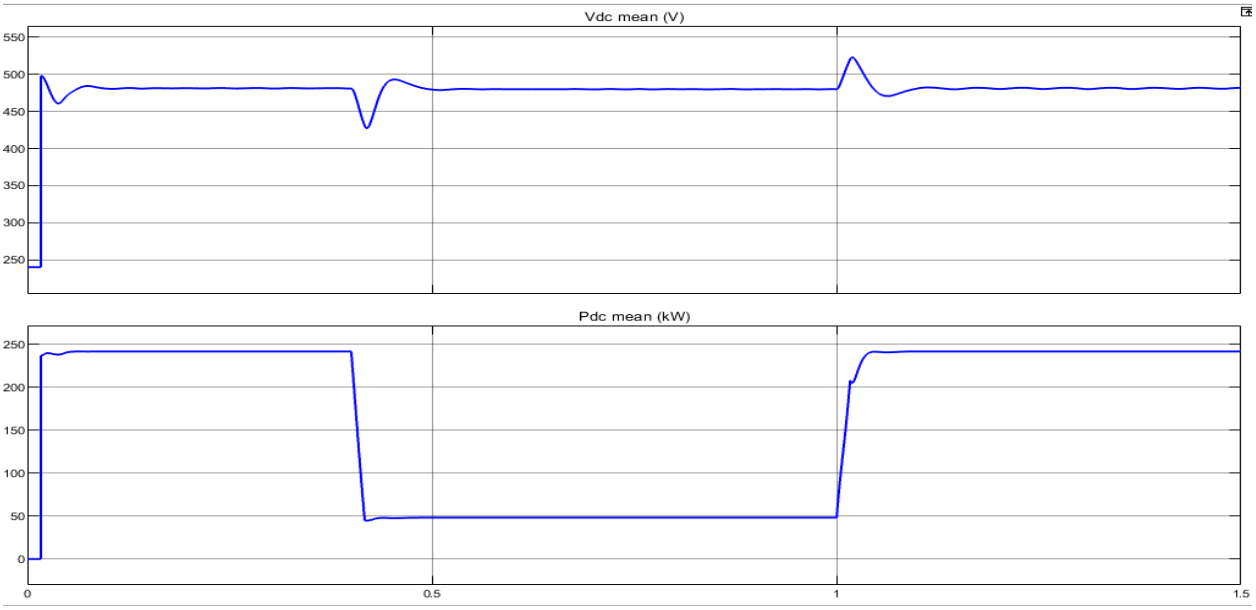

Figure 4. 7: Simulation results of output dc voltage and dc power from the PV solar with P&O based MPPT controller

The output of a system's mean DC voltage (Vdc) and mean DC power (Pdc) are plotted in two different ways in the result. As input circumstances fluctuate, the mean DC voltage, which is depicted in the upper plot, shows brief dips and rises but mainly stays constant between 470 and 490V. As seen in Figure 4.7, the mean DC power in the lower plot exhibits stepped changes that clearly correspond to variations in the input irradiance, most likely reflecting the reaction of a P&O MPPT controller.

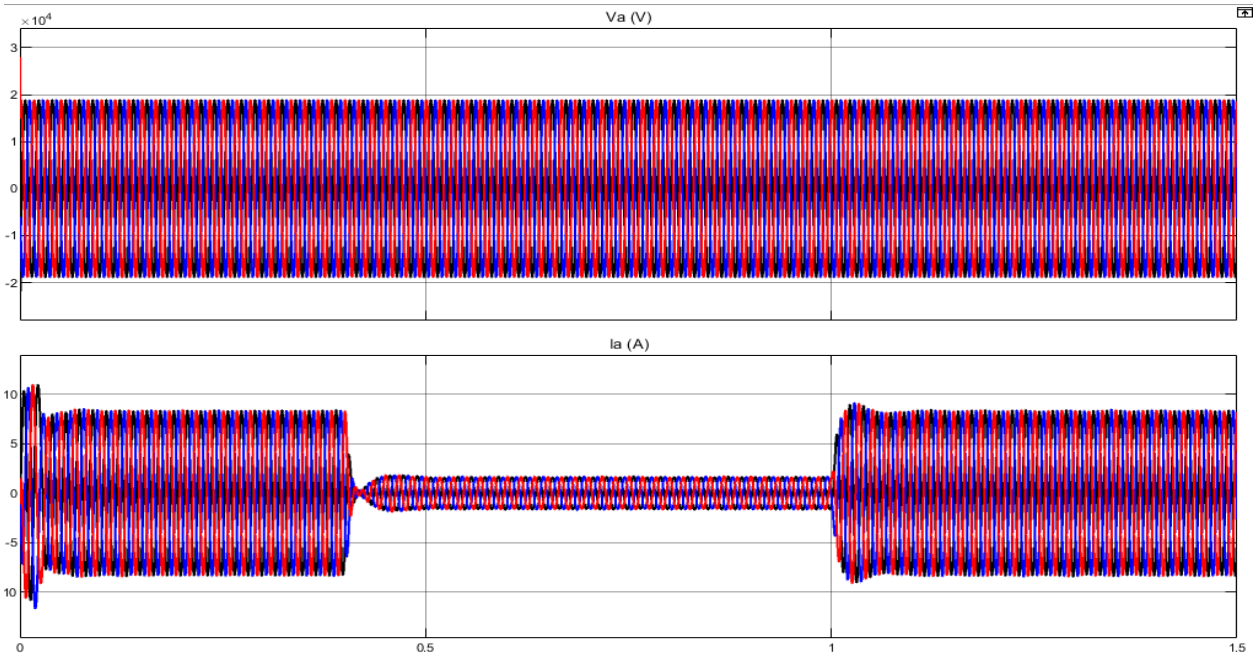

Figure 4. 8: AC voltage and current simulation results using the MPPT P&O controller

The two graphs in Figure 4.8 show the instantaneous voltage (Va) and current (Ia) waveforms, and they are most likely from the AC side of the inverter in the water pumping system. Continuous sinusoidal oscillations with a relatively constant amplitude are displayed in the top plot for Va (Voltage), whereas the bottom plot for Ia (Current) shows significant changes in amplitude, especially a sharp drop around 0.4 seconds and a corresponding increase around 1.0 seconds, which reflect variations in the system's load or power output.

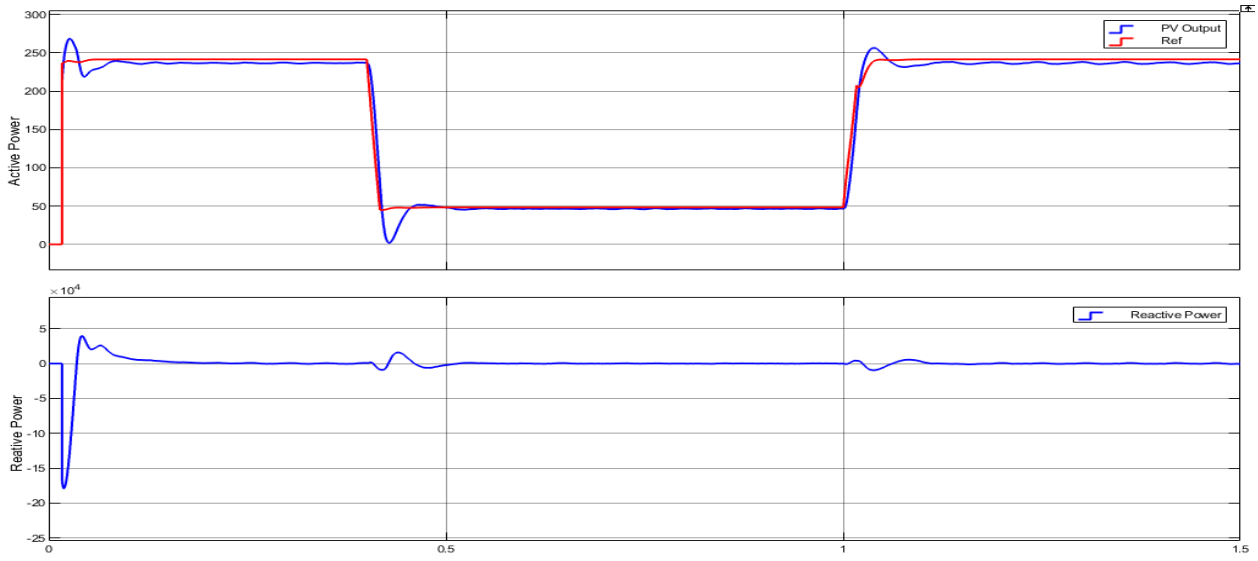

Figure 4. 9: Output power simulation results using the MPPT's P&O controller

The simulations in Figure 4.9 display the output power of a PV system controlled by a P&O MPPT algorithm. In the top figure, which shows the active power, the "PV Output" (blue line) closely tracks the "Ref" (reference) power (red line). The active power starts out at about 240 kW, drops down to about 50 kW after 0.4 seconds, and then rises again to about 240 W after 1.0 seconds. This dynamic response, which mimics the irradiance variations seen in Figure 4.6, amply illustrates the MPPT's capacity to extract power that reacts to stepwise changes in environmental conditions. The reactive power, which is shown in the bottom figure and stays close to 0 Var with only little variations, shows that the system mostly provides active power.

Two MPPT controllers, ANFIS and P&O, are directly compared based on important solar PV system parameters in Table 4.1: Comparison result of ANFIS and P&O for MPPT. While P&O obtains 240 kW for Maximum Power (Pmax), ANFIS achieves 270 kW, suggesting a higher power output with ANFIS. In line with this, ANFIS's voltage (V) is 480 V as opposed to P&O's 475 V, and its current (I) is 10 A as opposed to P&O's 9.5 A. In terms of obtaining the most electricity possible from the PV system, this data indicates that ANFIS performs better than P&O.

Table 4. 1: Comparison result of ANFIS and P&O for MPPT

	MPPT controllers

System parameters of solar PV	ANFIS	P&O
Pmax (kW)	270	240
Voltage (V)	480	475
Current (I)	10	9.5

4.5 Simulation results of PMSM with FOC based speed control

The following simulation results are obtained using the mechanism of FOC of induction machine.

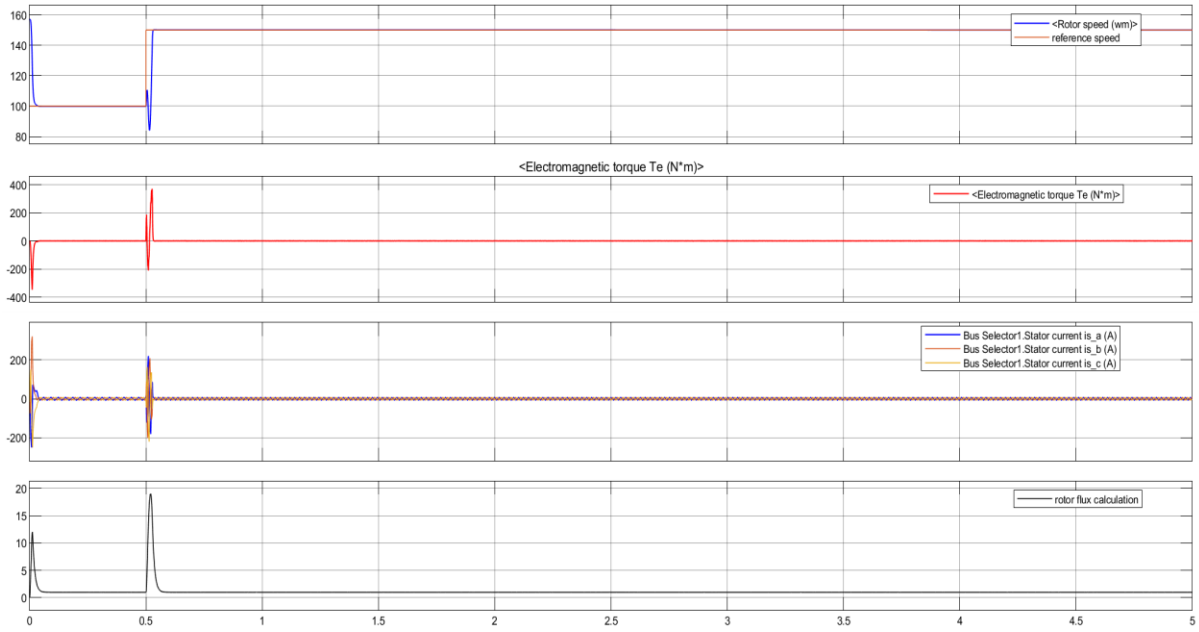

Figure 4. 10: Rotor speed, torque, stator current, and rotor flux simulation results for PMSM using an outer loop controller

When the induction motor is operating at a reference speed of 100 rad/s for 0.5 seconds, the response settles at 17.2 ms, demonstrating that the PI controller can rapidly reach a steady state and has superior tracking performance for the speed control of indirect vector-controlled induction motor drives (Figure 4.10).

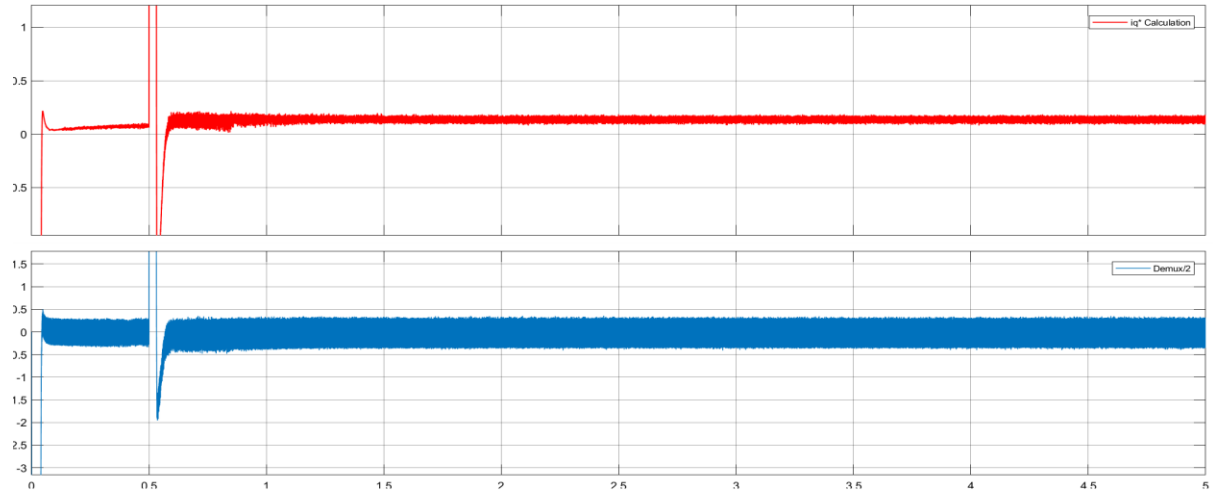

Figure 4. 11:Iq and Iq* simulation results of FOC PMSM

Figure 4.11 indicates that the Iq just follows Iq* (command current) in a speed control trajectory Overall simulation Simulink diagram shown in figure 4 is the FOC of induction machine with inner and outer loop controller.

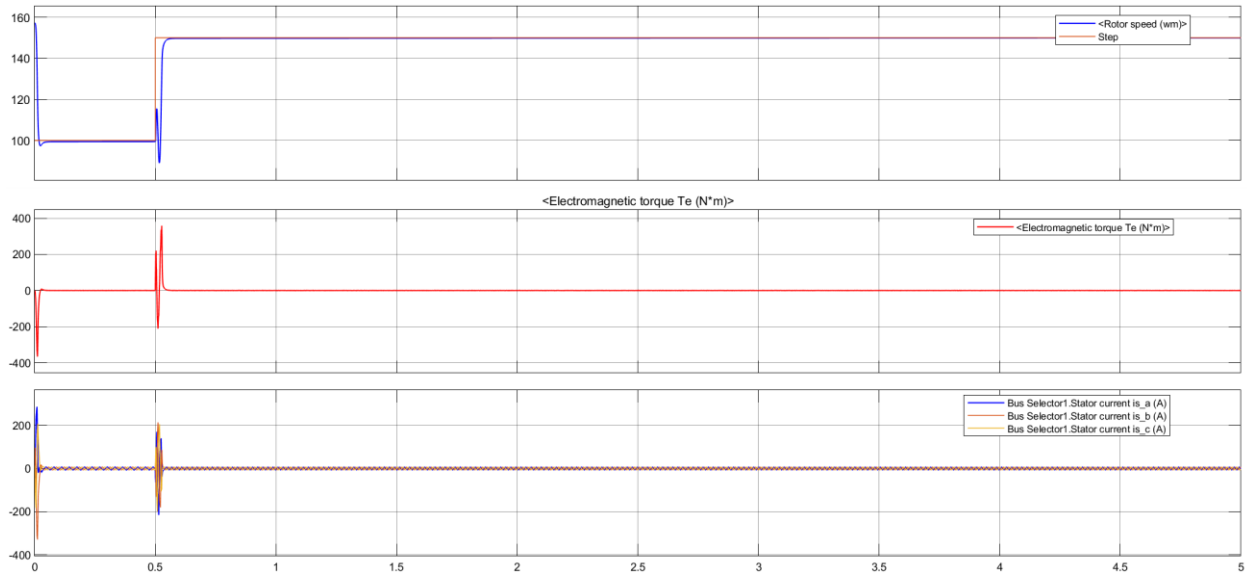

Figure 4. 12: Simulation responses for inner current loop

Figure 4.12 shows the speed and torque response while maintaining all other parameters constant and adding an inner current controller. As can be seen, there is no overshoot in speed response and the setting time is lowered to 11.7 ms.

CHAPTER 5
CONCLUSIONS AND RECOMMENDATIONS

5.1 Conclusions

This thesis successfully introduced and evaluated an Adaptive Neuro-Fuzzy Inference System (ANFIS) as a dependable and efficient replacement for traditional P&O controllers for MPPT in a solar PV-powered PMSM drive for irrigation The comprehensive simulations performed in MATLAB/Simulink validate the efficacy of the proposed ANFIS controller. The primary finding of the study is that power extraction has greatly improved. Peak power production of 270 kW was produced using the ANFIS-based MPPT, a significant 12.5% increase over the 240 kW obtained with the P&O method. This increased power is closely connected with higher voltage delivery at 480 V and current at 10 A, indicating the controller's ability to maintain the PV system closer to its true maximum power point.

For efficient irrigation applications, a steady and amplified power supply is necessary, and the ANFIS controller also aids in greatly lowering harmonic distortions and accelerating system response times. ANFIS's potential to improve motor drives driven by renewable energy for vital agricultural operations is demonstrated by the enhanced performance.

5.2 Recommendations

The following suggestions are made for further study and use in light of the successful simulation findings and the proven benefits of the ANFIS-based control strategy:

- A physical prototype of the proposed ANFIS-controlled PV-PMSM pumping system should be constructed. This will make it possible to empirically test the modeling results including the dynamic response and harmonic performance under actual fluctuations in load circumstances, temperature, and sun irradiation.
- Conduct a detailed techno-economic feasibility study comparing the ANFIS-PMSM system with conventional diesel pumps and other electric pumping solutions in the Ethiopia.

- While ANFIS showed promising results, further research could explore and compare its performance with other advanced AI techniques (e.g., Deep Learning, Reinforcement Learning) or hybrid optimization algorithms for even greater efficiency and resilience.

REFERENCES

"Engineering ToolBox. Hydraulic Diameter. (2019.). ,"*https://www.engineeringtoolbox.com/hydraulic-equivalent-diameter-d_458.html*,.

DC to DC converter pdf,. ([Accessed 11, 02, 2023].). *Online4, https://core.ac.uk/download/pdf/61802295.*

Gursoy, M.; Zhuo, G.; Lozowski, A.G.; Wang, X. (2021). *Photovoltaic Energy Conversion Systems with Sliding Mode Control. Energies , 14, 6071. https://doi.org/10.3390/en14196071*.

A. Abubakar and S. Paulo. (no. August 2023). "A Review of Solar Photovoltaic System Maintenance Strategies,". *doi: 10.1109/INDUSCON51756.2021.9529669.*

A. Halmous, Y. O. (2024). "Techno-Economic Study of Grid-Connected Hybrid Renewable Energy Systems Optimized by Homer Pro," 2024 2nd Int. Conf. Electr. Eng. Autom. Control,. , *doi: 10.1109/ICEEAC61226.2024.10576327.*, pp. 1–6, .

Aklilu, H. B. (june 2023). Modeling and Control of a Standalone Photovoltaic Using Fuzzy Based Perturb and Observe Maximum Power Point Tracking Controller for Water Pumping Application: (Case Study at Koka, Ethiopia). *Adama Science and Technology University Master Thesis in Electrical power*.

Al-Ezzi, A. S. (2022). Photovoltaic Solar Cells: A Review. Applied System Innovation,. *https://doi.org/10.3390/asi5040067*, 5(4), 67.

Ali ME, A. Y. (2020). Modern Maximum Power Point Tracking Techniques for Photovoltaic Energy Systems. Green Energy and Technology. *Green Energy and Technology. Cham: Springer.*

E. E. Hsduwphqw, I. C. (2024). “Neurofuzzy Based MPPT for a Hybrid Powered BLDC Motor in Water Pumping Applications,” 2024 IEEE Third Int. Conf. Power Electron. Intell. Control Energy Syst.,, . *doi: 10.1109/ICPEI*, pp. 1155–1160.

EEP. (n.d.). *Power Generation*. (Ethiopian Electric Power) Retrieved Jun 17, 2021, from https://www.eep.com.et/en/power-generation/

Elssaify, R. &. (2024). Types of PV Solar Cell Models. *https://www.researchgate.net/publication/378402410_Types_of_PV_Solar_Cell_Models*.

G. P. Zhang. (2000). Neural networks for classification. *IEEE Transactions on Systems, Man, and Cybernetics, 30*(4), 451- 462.

I. Saady et al. (2025). “Improving photovoltaic water pumping system performance with ANN-based direct torque control using real-time simulation,” . pp. 1–28, .

K. Chnini, H. J. (2025,). “ANFIS-RTSMC based MPPT for a hybrid PV-diesel-battery water pumping system,” . *doi: 10.1177/00202940241277095.*, vol. 58, no. 6, pp. 711–727,.

Karim, I. S. (2025). “Performance Optimization of Photovoltaic Water Pumping Systems : A Comparative Study of PSO- Based and ANN-Based MPPT with Real-Time Validation,” 2025 7th Int. Congr. Human-Computer Interact. Optim. Robot. Appl., do. pp. 1–13, .

Karim, I. Saady and M. (2025). “Performance Optimization of Photovoltaic Water Pumping Systems : A Comparative Study of PSO- Based and ANN-Based MPPT with Real-Time Validation,” Congr. Human-Computer Interact. Optim. Robot. Appl.,. pp. 1–13, 2025.

Kenu E. sarah, U. R. (2020). A Review of Solar Photovoltaic Technologies. *INTERNATIONAL JOURNAL OF ENGINEERING RESEARCH & TECHNOLOGY (IJERT)* , Volume 09, Issue 07 .

Lee, J., Chae,W., & Kim, W. (2022). Control Strategy for Line Overload and Short Circuit Current of Networked Distribution Systems. *Sustainability, 14*.

M. Hassan, M. A. (March, 2022.). “Highly Efficient MPP Tracker Based on Adaptive Neuro-fuzzy Inference System for Stand-Alone Photovoltaic Generator System,” no.

Magaji, N. W. (2022). Application of Type 2 Fuzzy for Maximum Power Point Tracker for Photovoltaic System. 1–25.

Magaji, N. W. (2022). Application of Type 2 Fuzzy for Maximum Power Point Tracker for Photovoltaic System. 1–25.

Mesfin, S. B. (2025). “Solar - powered ANN - based MPPT with zeta converter for BLDC motor water pumping in rural Ethiopia for sustainable agriculture,” Discov. Sustain.,. *doi: 10.1007/s43621-025-00893-8.*

P. B. Biragbara, D. C. (2022). “Voltage Optimization of PV / Wind Hybrid Renewable Energy System using Adaptive Neuro-Fuzzy Logic Technique,” . vol. 4, no. 3, pp. 77–84, .

Ranjan, S., Jaiswal, S., Latif, A., Das, D., Sinha, N., Hussain, S., et al. (2021). Isolated and Interconnected Multi-Area Hybrid Power Systems: A Review on Control Strategies. *https://doi.org/10.3390/en14248276*.

Reddy, K. H. (2020). Modeling and Performance Analysis of Perturb and Observe (P & O), Incremental Conductance (IC), Fuzzy Logic.

Reddy, K. H. (2020). Modeling and Performance Analysis of Perturb and Observe (P & O), Incremental Conductance (IC), Fuzzy Logic.

Reddy, K. H., Vijayasanthi, R., & Ramasudha, K. (2020). Modeling and Performance Analysis of Perturb and Observe (P & O), Incremental Conductance (IC), Fuzzy Logic.

Revathy, S. (2022). Design and analysis of ANFIS–based MPPT method for solar photovoltaic applications. *International Journal of Photoenergy .1 (2022): 9625564*.

S. S. V Mohan, S. P. (2025). “Nature - inspired MPPT algorithms for solar PV and fault classification using deep learning techniques,” Discov. Appl. Sci.,. *doi: 10.1007/s42452-024-06446-4.*

U. Joshi, P. S. (22 June 2022). Advances in MeteorologyVolume 2022, Issue 1 .First published:.

Z. Boumous and S. Boumous. (2024). “Novel Intelligent control of photovoltaic system using ANFIS Gravitational Search for MPPT controller,”,. *doi: 10.15199/48.2024.07.22.*, no. 7, pp. 108–112, .

APPENDIX

Appendix: Overall Simulink diagram of the system

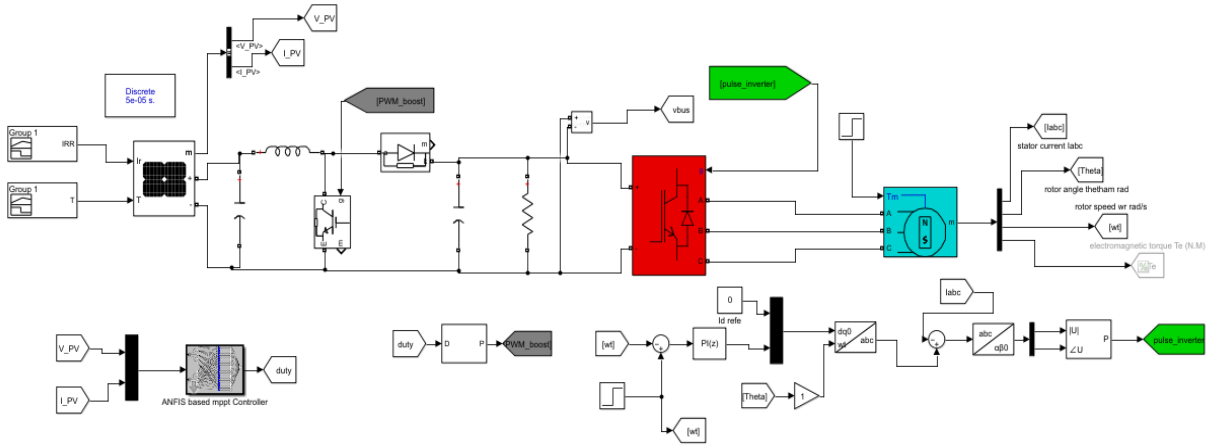

Simulink model of FOC PMSM

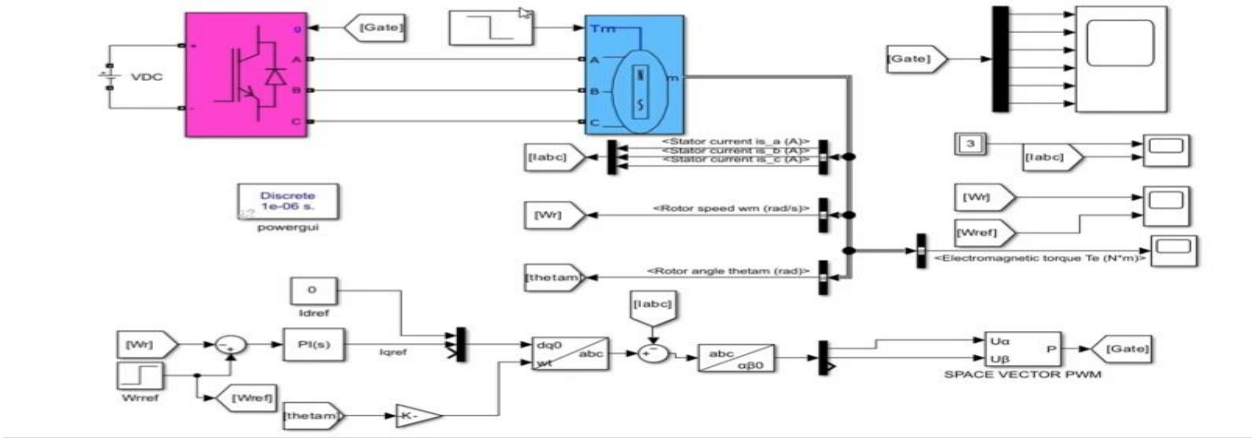

Figure 3.8: Simulink model of ANFIS based MPPT controller

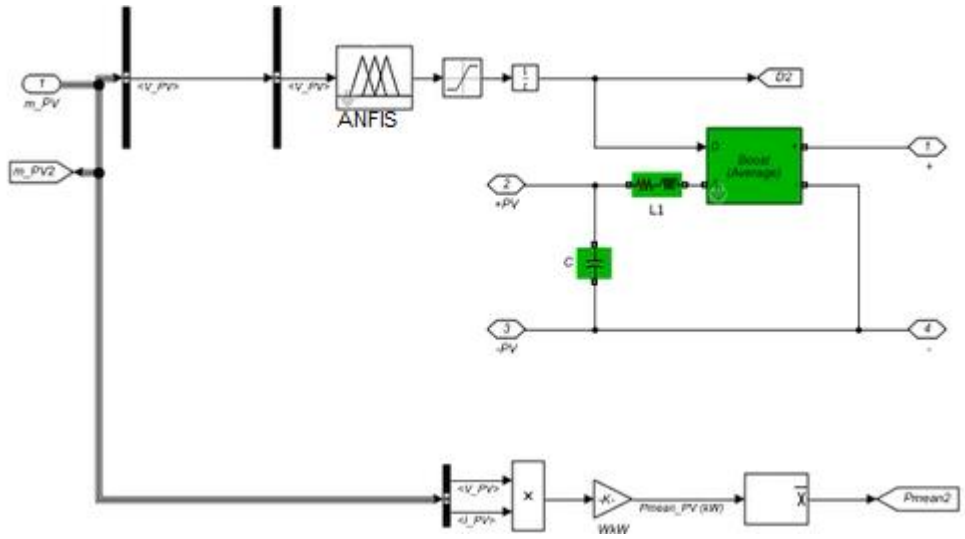

Figure 3.16: Simulink model of P&O algorithm with MATLAB function block diagram